DEBRIS DETECTION USING SMALL SATELLITES.

M.Tech Thesis

By:

Shubhi Tiwari

DEPARTMENT OF ASTRONOMY , ASTROPHYSICS AND SPACE ENGINEERING

INDIAN INSTITUTE OF TECHNOLOGY INDORE

May 16, 2025

DEBRIS DETECTION USING SMALL SATELLITES

A THESIS

Submitted in partial fulfillment of the
requirements for the award of the degree
of
M.Tech

by
Shubhi Tiwari

DEPARTMENT OF ASTRONOMY , ASTROPHYSICS AND SPACE ENGINEERING

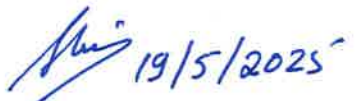**INDIAN INSTITUTE OF TECHNOLOGY INDORE**

May 16, 2025

INDIAN INSTITUTE OF TECHNOLOGY INDORE

CANDIDATE'S DECLARATION

I hereby certify that the work which is being presented in the thesis entitled **DEBRIS DETECTION USING SMALL SATELLITES** in the partial fulfillment of the requirements for the award of the degree of **MASTER OF TECHNOLOGY** and submitted in the **DEPARTMENT OF ASTROPHYSICS, ASTRONOMY AND SPACE ENGINEERING, Indian Institute of Technology Indore**, is an authentic record of my own work carried out during the time period from July 2023 to May 2025 under the supervision of Dr. Abhirup Datta, Professor, Indian Institute of Technology Indore and Dr. Hari B Hablani, Professor, Indian Institute of Technology Indore.

The matter presented in this thesis has not been submitted by me for the award of any other degree of this or any other institute.

19/5/2025

**Signature of the student with date
(SHUBHI TIWARI)**

This is to certify that the above statement made by the candidate is correct to the best of my/our knowledge.

Hari Hablani

Signature of the Supervisor of
M.Tech. thesis (with date)

Prof. Hari B. Hablani
May 19, 2025

Signature of the Supervisor of
M.Tech. thesis (with date)

Prof. Abhirup Datta

Shubhi Tiwari has successfully given his/her M.Tech. Oral Examination held on **6th May 2025**.

Hari Hablani

Signature(s) of Supervisor(s) of MTech thesis
Date: May 19, 2025

Manonita Chakraborty

Convenor, DPGC
Date: 16/05/2025

Programme Coordinator, M.Tech.
Date: 16-05-2025

HoD, DAASE
Date:

ACKNOWLEDGEMENT

ABSTRACT

CubeSats are compact, cost-effective satellites that have revolutionized space exploration and research. Their smaller size and shorter development life cycle make them an attractive choice for a wide range of missions, particularly for scientific studies and technology demonstrations. These satellites are modular in design and can be tailored to meet specific mission requirements, offering unprecedented flexibility in space research. CubeSats are particularly well-suited for addressing the growing challenge of space debris detection due to their adaptability and ability to host advanced sensing technologies within a compact framework.

Space debris encompass waste from different sources such as defunct satellites, spent rocket stages, or cosmic. They can be fatal to resident space objects. Following the design and operation of Space-Based Visible, we aim to design an infrared-visible space-based sensor to detect, track and determine the orbits of space debris in the 1-10cm range in the LEO environment. The infrared-visible sensor is hosted on an inertially stabilized satellite in a dawn-dusk sun-synchronous orbit. The sensor measures the right ascension α_d and declination δ_d angles of a debris. The sunrays illuminate the debris at a time-varying phase angle. The debris when above the horizon of the spacecraft and within the field of view of the sensor aperture will streak across the focal plane. We have explored sidereal tracking, in which the focal plane is inertially stabilized and this work will lay grounds for exploring ephemeris tracking, in which the sensor tracks the debris to gather sufficient measurements.

The integration of compact and efficient components ensures that the CubeSat can operate autonomously and reliably in the harsh conditions of space. By advancing our capability to monitor and study space debris, this project aims to contribute significantly to global efforts in space sustainability and the development of safer orbital operations.

In this study, a discussion about the satellite's orbit and the sensor's control to identify the debris is compiled.

Contents

List of Figures

Chapter 1

Introduction

Space debris is a viable concern in Earth's orbital environment. It comprises inactive satellites, dead rocket stages, and fragments from collisions or disintegration events. With tens of thousands of tracked objects and millions of smaller fragments, the risk of collisions in orbit has escalated significantly, threatening operational satellites, spacecraft, and even the International Space Station. Addressing this issue is critical for maintaining the sustainability of space operations and enabling future advancements in space exploration and satellite technology.

CubeSats, a class of small, standardized satellites, have emerged as a cost-effective and innovative solution for space debris detection and monitoring. With their compact size, modular design, and affordability, CubeSats offers a scalable platform for deploying sensors and communication systems to detect, track, and analyze orbital debris.

Equipped with technologies such as radar systems, optical sensors, and LiDAR, CubeSats can detect and characterize debris ranging from larger objects to smaller, high-risk fragments. Advances in miniaturized electronics and onboard data processing have enhanced the capabilities of CubeSats, allowing them to perform sophisticated tasks despite their size and resource constraints.

1.1 Debris in Space

Space debris, also known as orbital debris or space junk, refers to non-functional, human-created objects that remain in Earth's orbit.This includes a variety of items such as defunct satellites, dead rocket stages, and fragments generated from collisions or disintegration events. With the growing commercialization and exploration of space, the volume of debris has steadily increased, presenting a significant challenge to the safety and sustainability of orbital operations.

Figure 1.1: Representation of Human made-Space Debris

1.1.1 Classification of Space Debris

Scientific models estimate the amount of space debris in Earth's orbit to be vast and varied based on size. There are roughly 29,000 objects larger than 10 cm, around 670,000 fragments exceeding 1 cm, and more than 170 million particles greater than 1 mm in diameter. Each of these debris pieces, regardless of size, poses a threat to active spacecraft due to their high orbital velocities. A collision with a fragment larger than 10 cm could cause the catastrophic breakup of a satellite, producing even more debris. Objects around 1 cm in size are capable of disabling spacecraft and even penetrating protective shields like those on the International

Space Station (ISS). Even smaller fragments, as tiny as 1 mm, have the potential to damage critical subsystems on spacecraft, such as solar panels or communication instruments. These risks highlight the urgent need for effective debris tracking and mitigation measures to safeguard orbital operations.

Debris Size	Similar in size to	Mass (g) aluminum sphere	Kinetic Energy (J)	Equiv. TNT (kg)	Energy similar to	Quantity	Trackable
1 mm	medium-grit sand or poppy seeds	0.0014	71	0.0003	Pitched baseball	Tens of millions	Can't be tracked
3 mm	smaller than BBs	0.038	1910	0.008	Bullets	Millions	Can't be tracked
1 cm	blueberries	1.41	70700	0.3	Falling anvil	Hundreds of thousands	Can't be tracked
5 cm	plum	176.7	8840000	37	Hit by bus	Tens of thousands	Most can't be tracked
10 cm	softball	1413.7	70700000	300	Large bomb	Tens of thousands	Most can be tracked
> 10 cm	basketball to football field	1400 to 500,000,000	Up to 1x10^13	Up to 3,000,000	Very large bomb	Thousands	Tracked and cataloged by the space surveillance network

Figure 1.2: Debris Size and Trace ability

Chapter 2

Literature Survey

2.1   Space Surveillance Mission

- **Geosynchronous Space Situational Awareness Program (GSSAP)** The Geosynchronous
  Space Situational Awareness Program (GSSAP) is a critical U.S. Space Command initia-
  tive designed to enhance space surveillance capabilities. Operating in the near-geosynchronous
  orbit regime, GSSAP satellites function as dedicated sensors for the Space Surveillance
  Network (SSN). Their primary role is to track, monitor, and analyze artificial objects
  in orbit, providing precise data for orbital predictions and ensuring spaceflight safety.
  Positioned strategically, these satellites enjoy an unobstructed view of Resident Space
  Objects (RSOs), free from the limitations of weather or atmospheric distortion that often
  affect ground-based systems.

  A significant feature of GSSAP is its ability to perform Rendezvous and Proximity Op-
  erations (RPO), which allows the satellites to maneuver close to objects of interest. This
  capability supports anomaly investigations and detailed characterization of RSOs, aiding
  in anomaly resolution, enhanced surveillance, and improved situational awareness while
  maintaining operational safety. The insights gathered by GSSAP are crucial for timely
  orbital adjustments and collision avoidance, contributing to a safer geosynchronous orbit
  environment.

Developed by Northrop Grumman, GSSAP operates at an altitude of approximately 22,300 miles (35,970 kilometers), providing a unique vantage point for monitoring the geosynchronous belt. By advancing space situational awareness, GSSAP plays a pivotal role in safeguarding critical assets in geosynchronous orbit and maintaining the security of U.S. space operations.

- **Space Situational Awareness (SSA)** The European Space Agency (ESA) is actively advancing its Space Situational Awareness (SSA) program to monitor and address risks in Earth's orbital environment. Launched in 2009, ESA's SSA initiative focuses on safeguarding vital space assets, ensuring operational safety, and mitigating potential hazards stemming from space debris, solar activity, and near-Earth objects (NEOs). This comprehensive approach underlines Europe's commitment to sustainable and secure operations in space.

  ESA's SSA framework is built on three key segments: Space Weather (SWE), Near-Earth Objects (NEO), and Space Surveillance and Tracking (SST). The SWE component involves monitoring solar activities and their effects on Earth's magnetosphere, ionosphere, and technological systems. This helps predict disruptions to satellites, communication systems, and power grids. The NEO segment focuses on identifying and tracking asteroids or comets that pose potential collision risks with Earth. ESA's dedicated NEO Coordination Centre provides critical data and forecasts to mitigate impact threats.

  In the SST domain, ESA monitors operational satellites, space debris, and defunct spacecraft to prevent collisions and ensure safe navigation in Earth's increasingly congested orbital regions. The establishment of ground-based radar and optical telescopes enables ESA to catalog and track thousands of objects, providing vital data for collision avoidance maneuvers. The Flyeye telescope, an advanced wide-field optical telescope, exemplifies ESA's cutting-edge technology in improving object detection capabilities.

  Notable projects under SSA include ESA's ClearSpace-1, a mission aimed at actively removing defunct satellites, demonstrating Europe's leadership in tackling space debris.

In addition, ESA collaborates with international partners to share data, foster innovation, and create a globally coordinated response to orbital threats.

- **Space Maitri: India's Vision for Space Debris Management** Space Maitri: India's Vision for Space Debris Management

Space Maitri is a conceptual initiative by India to address the growing challenge of space debris management and sustainability in orbit. As global concerns about orbital congestion increase due to the proliferation of satellites and space missions, Space Maitri aims to position India as a leader in mitigating the risks associated with space debris. The program emphasizes developing indigenous technologies to detect, track, and remove debris from Earth's orbital environment while fostering international collaboration.

The proposed mission seeks to integrate advanced debris removal technologies such as robotic arms, nets, and drag-enhancing sails to capture and deorbit defunct satellites and other debris. These innovations aim to ensure that India's satellites and global assets in orbit remain safe from collisions. Space Maitri also focuses on building artificial intelligence (AI)-driven data fusion systems to enhance space situational awareness (SSA) capabilities, enabling real-time tracking and prediction of debris trajectories for collision avoidance.

India's Space Research Organisation (ISRO) has already laid the groundwork for Space Maitri through its Project NETRA, which is developing a robust surveillance network to monitor space debris. Space Maitri builds on this foundation, aiming to take a more proactive role in removing debris from critical orbital regions, especially low Earth orbit (LEO) and geosynchronous orbit (GEO).

By aligning with global debris management standards and fostering international partnerships, Space Maitri embodies India's commitment to sustainable space operations. It aims to protect the orbital environment for future generations and support India's growing role in space exploration and commercialization. Space Maitri seeks to contribute to the global effort in maintaining the safety and sustainability of space for all.

2.2 CubeSat Introduction

CubeSats, a category of nanosatellites, adhere to a standardized size and form factor. The conventional CubeSat dimensions are denoted as"1U" or one unit," measuring 100 mm x 100 mm x 100 mm, and can be scaled to larger sizes, including 1.5U, 2U, 3U, 6U, and even 12U (Fig. 2.1). Originating in 1999 through collaborative efforts by California Polytechnic State University at San Luis Obispo (Cal Poly) and Stanford University, CubeSats were initially designed to serve as a versatile platform for educational purposes and space exploration. Over time, the development of Cube-Sats has evolved into a distinct industry, with active collaboration among government entities, industries, and academic institutions, resulting in continually expanding capabilities. CubeSats have emerged as a cost-effective solution for conducting scientific investigations, showcasing new technology, and implementing advanced mission concepts, such as constellations, swarms, and modular systems.[1].
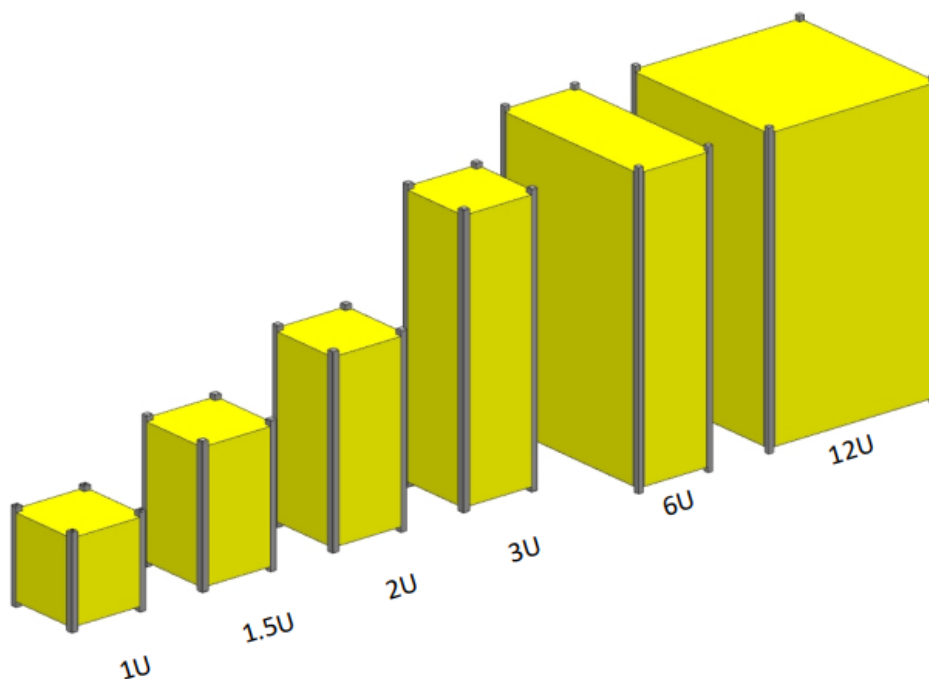
Figure 2.1: CubeSat Family [1]

2.2.1   India's CubeSat Missions

Below are some CubeSat missions by India :

STUDSAT

STUDSAT is a 1U picosatellite successfully launched into a Sun-synchronous orbit on July 12, 2010, from the Satish Dhawan Space Centre. The mission's objective was for students to gain practical experience in the design, manufacture, and implementation of a low-cost space mission.
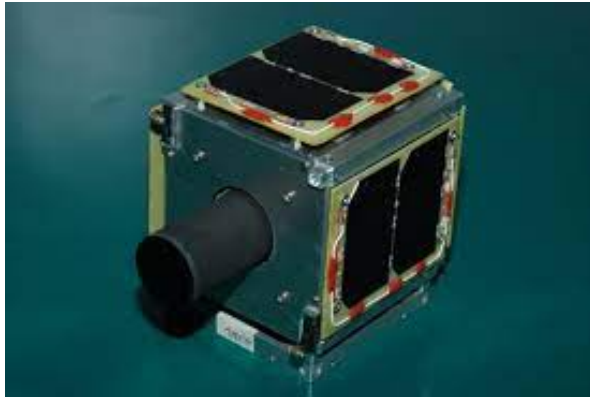
Jugnu

Jugnu is a 3U CubeSat that was utilized for technological demonstration and remote sensing. The Indian Institute of Technology Kanpur ran it. On October 12, 2011, PSLV-CA C18 launched Jugnu into low Earth orbit.
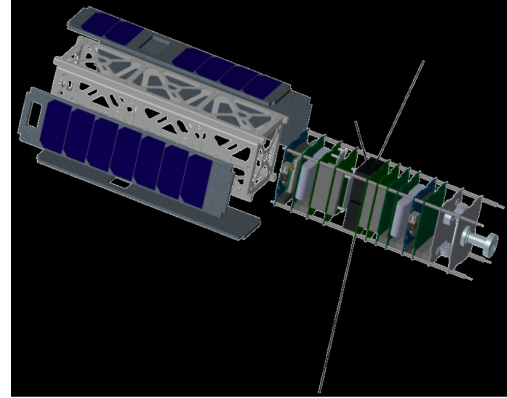
Swayam

Students from the College of Engineering in Pune built the tiny satellite, Swayam, a 1U-sized CubeSat. On June 22, 2016, ISRO launched it into space from the Satish Dhawan Space Center in Sriharikota, India, atop the Polar Satellite Launch Vehicle C-34, along with Cartosat-2C.
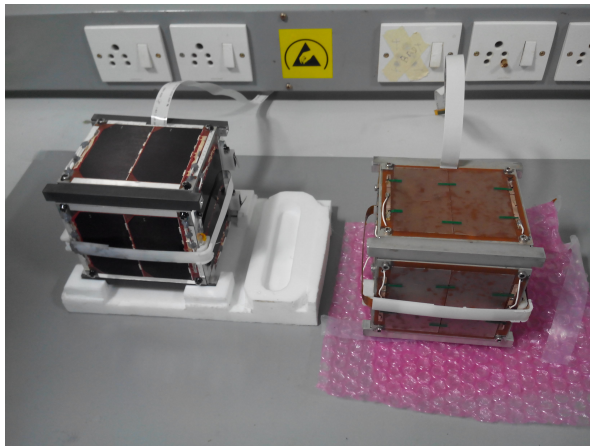
Pratham

The 1U satellite Pratham was created for Indian ionospheric research. Under the Student Satellite Initiative, it was run by the Indian Institute of Technology Bombay. Its primary objective is to count the electrons in the ionosphere of Earth. The cube-shaped Pratham is 30 centimeters on each side and weighs about 10.15 kilos. Along with seven other satellites on a PSLV C-35, it was successfully launched on September 26, 2016, from the Satish Dhawan Space Centre in Sriharikota, Andhra Pradesh.

(a)   (b)

(c)   (d)

Figure 2.2: (a) STUDSAT (b) Jugnu (c) Swayam (d) Pratham

2.3   CubeSats for Space Debris Study

In this section development of CubeSats for Space Debris Detection are discussed.

- **ADCS development for student CubeSat satellites** The paper discusses two student satellites and their approach to Attitude Determination and Control Systems (ADCS) with a focus on debris removal. The TTU100 satellite requires an ADCS to meet various mission objectives, particularly for pointing the cameras and X-band radio towards specific targets. The system must be able to detumble the satellite, reducing its spin rate from ±50°/s to ±0.15°/s (with two spins per orbit) within seven days. The system also needs to meet specific pointing accuracy requirements: 45 degrees for the UHF communication system, 10 degrees for the X-band communication system, and 3 degrees for both the camera system and the laser communication experiment. Additionally, the ADCS

should allow for remotely configurable parameters and provide real-time status updates for all sensors and control loop states. Remote programming is essential, ensuring that an incomplete programming sequence does not prevent new progra-mming attempts and that the software responsible for monitoring the health of the primary software image is not overwritten. The primary operating modes of the ADCS include detumbling, which slows high rotational speeds post-launch to enable the transition to standard control algo-rithms; Y-Thomson spin, where the satellite's spin axis aligns with the orbital axis, keep-ing one point of the satellite consistently pointed toward the Earth; tracking geographical points for image capture; and sun pointing, which ensures the satellite is oriented to maximize power harvesting from the Sun.[7]

- **Mission design and Guidance, Navigation, and Control systems for in-orbit demon-stration of Active Debris Removal technologies using CubeSats.** The study addressed several challenges related to in-orbit debris removal, focusing on demonstrating scalable solutions for large debris removal operations. It explored the potential of CubeSats to op-erate in the Active Debris Removal (ADR) environment, validating the technology and providing a downsized platform for demonstrating this capability. The mission design and Guidance, Navigation, and Control (GNC) systems were developed to support ADR experiments.

  The paper proposes the Chaser-Target approach, which involves identifying the geom-etry, texture, and motion of the target, as well as incorporating collision avoidance and capture concepts. This approach also requires validation of inter-ception points and syn-chronization with the target before capture. To achieve this, 2D-3D sensors, data fusion algorithms, and GNC algorithms are necessary. The Ballistic Coefficient Ratio between the chaser and target was adjusted to reduce the drag coefficient mismatch.

  The study identifies several key performance indicators, including Line of Sight (LoS), operational distance, relative speed, permanent target visibility, point cloud generation quality, data latency, sensor accuracy against spacecraft vibrations, power consumption,

scalability for both large-scale and CubeSat ADR missions, and range accuracy. For detection, a single wide-beam X-band radar was used for far/medium range scanning, combined with an IR camera to enhance the measurements. [2]

- **Debris Detection Using Star Tracker Concept Verification** This research explores using a star tracker for detecting and tracking space debris. Traditionally, star trackers are used to determine a spacecraft's orientation by identifying stars in its field of view. However, the authors repurposed this technology to also identify and track space debris. The process begins by detecting bright blobs in the images captured by the star tracker. These blobs, which could be either stars or debris, are processed using a centroiding algorithm that determines their center.

  The key innovation in this approach is the use of a Kalman filter to track these detected blobs over time, helping reduce measurement errors and noise. The filter combines predicted object positions based on spacecraft motion with actual measurements to estimate the true location of the objects. The objects' velocities are calculated and compared: stars, which are far away, move predictably, while space debris, being closer, exhibits more erratic motion. If an object's velocity deviates significantly from the typical motion of stars, it is flagged as debris.

  The star tracker system was tested on the Mercator telescope in La Palma, where real night sky tests were conducted. Despite not being designed for debris tracking, the Sagitta star tracker successfully identified space debris during the tests. The detected objects were further analyzed to determine their orbit. One of the identified debris objects was the SUZAKU satellite, which had ceased functioning and was now classified as space debris.

  In conclusion, this study demonstrates that star trackers can be adapted for space debris detection and tracking, offering a potential method for space traffic management. By using existing star tracker algorithms with slight modifications, the computational load is reduced, making it a viable solution for tracking space debris in real time.[5]

Chapter 3

Methodology to Scan Space

The project focuses on tracking debris in the in-situ space environment. The primary goal is to develop a system capable of detecting and differentiating space debris from other objects, such as stars. Key components of the project include the development of a bi-axis gimbaled sensor station, which will allow for precise scanning and tracking of objects in the space environment. To achieve accurate debris tracking, the system will utilize optical sensors to observe the debris, capturing scattered waves from objects to help quantify the debris relative to stars.

An important aspect of the project is the creation of an algorithm designed to differentiate between space debris and stars. This will allow the system to classify observed objects correctly. The data collected will then be downlinked to facilitate orbit determination, providing essential information for accurate tracking.

Once the data is obtained, the resulting orbits will be plotted using Systems Tool Kit (STK) software. By comparing the predicted orbits against known star positions, the system can effectively reject or accept an object as space debris. This methodology ensures that only genuine debris is classified as such, enabling more precise monitoring of the space environment.
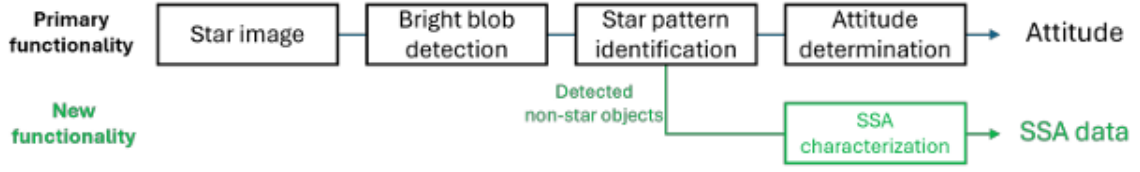
Figure 3.1: Workflow of Star Tracker
[5]

3.1 Mission Profile

- **Satellite's Orbit** The mission aims to study and scan Space Environment to study debris lesser than 10cm, by placing a CubeSat at 720km altitude away from Earth as The debris lesser than 10cm is mostly present at 800Km altitude. The Satellite will be a sun-synchronous satellite, with e=0 and inclination angle as 98.3°. The calculation is as follows: The rate of change of the right ascension of the ascending node is given by [3]:

$$\dot{\Omega} = -\frac{3}{2} J_2 \left(\frac{GM}{a^3} \right)^{-\frac{1}{2}} \left(\frac{Re}{p} \right)^2 \cos i \tag{3.1}$$

Given Data:

- **Earth's equatorial radius** (R_E):

$$R_E = 6378 \,\text{km} \tag{3.2}$$

- **Satellite altitude** (h):

$$h = 720 \,\text{km} \tag{3.3}$$

- **Semi-major axis** (a):

$$a = R_E + h = 6378.137 + 720 = 7098.137 \,\text{km} \tag{3.4}$$

- **Orbital eccentricity** (e):

$$e = 0 \quad \text{(assuming a circular orbit)} \tag{3.5}$$

- **Gravitational constant** (μ):

$$\mu = 398600.4418 \, \text{km}^3/\text{s}^2 \tag{3.6}$$

- **Oblateness coefficient** (J_2):

$$J_2 = 1.08263 \times 10^{-3} \tag{3.7}$$

Calculation of Inclination Angle (i):

Given the equation:

$$\dot{\Omega} = -\frac{3}{2} J_2 \left(\frac{GM}{a^3} \right)^{-\frac{1}{2}} \left(\frac{Re}{p} \right)^2 \cos i \tag{3.8}$$

we substitute the values:

$$\dot{\Omega} = 0.9856° \text{ per day},$$

$$J_2 = 1.08263 \times 10^{-3},$$

$$R_E = 6378.137 \, \text{km},$$

$$a = 7098.137 \, \text{km},$$

Rearranging for $\cos i$:

$$\cos i = \frac{-\dot{\Omega}}{-\frac{3}{2} J_2 \left(\frac{GM}{a^3} \right)^{-\frac{1}{2}} \left(\frac{Re}{p} \right)^2} \tag{3.9}$$

Substituting the known values:

$$\cos i = \frac{(0.9856)}{\frac{-3}{2}(1.08263 \times 10^{-3}) \left(\frac{398600.4418}{7098.137^3} \right)^2 \frac{6378.137}{7098.137}}. \tag{3.10}$$

Thus, the inclination angle i is calculated as:

$$i = \cos^{-1}(-0.12186) = 98.2667 \text{ degrees.} \tag{3.11}$$

- **Sun-Synchronous Satellite** A sun-synchronous satellite in a twilight orbit will help the satellite harness the maximum sun's energy. The twilight orbit is a polar orbit. When placed in a dawn-dusk Sun-synchronous orbit, the satellite moves along the line where the Earth transitions from night to day. The Keplerian orbit rate is 0.0011 rad/sec, 5226.3 deg/day. The sun-synchronous satellite has a property that it comes back to its original longitude (it repeats) from where it started. In the figure 3.3 illustrated below the yellow markers are the day one markers and the purple markers are the day two markers, the gradual increase in the length of the markers shows that the incremental orbit, as illustrated the satellite starts from -24.8275 degree longitude after 99.31 minutes it crosses -49.655 degree longitude. In a day the satellite orbits 14.5 times and in 2 days the satellite orbits 29 times.

$$n_{1,\text{kep}} = \left(\frac{\mu_E}{\text{a}^3} \right)^{0.5} \tag{3.12}$$
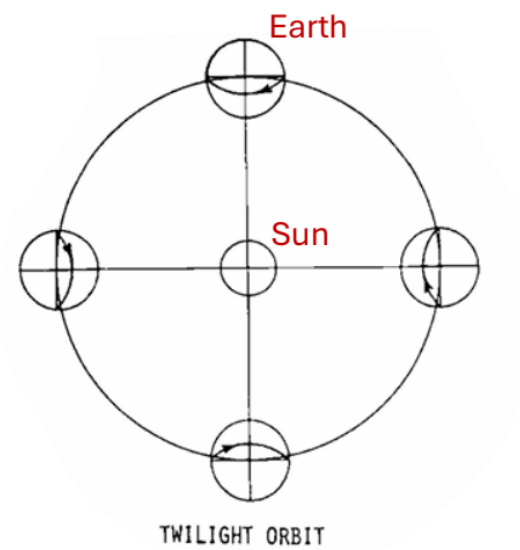
Figure 3.2: Twilight Orbit

[3]
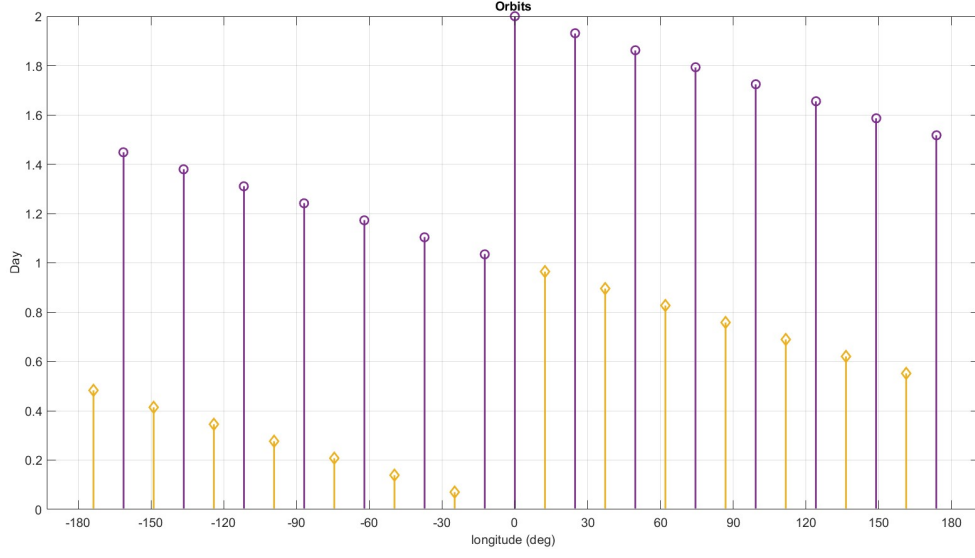
Figure 3.3: Orbits and longitude

- **Draconic Orbit** The attitude is selected in such a way that the debris tracking is repeated after some specified days and orbits. Here one orbit refers to the time between two subsequent nodal crossings, which is known as the draconic orbit period.The draconic period is 99.31 minutes.

$$\omega = -0.75 \, n_{1,\text{kep}} \, J_2 \left(\frac{R_{\text{eq}}}{\mathbf{a}} \right)^2 (1 - 5 \cos^2 i) \qquad (3.13)$$

$$\Delta n = -0.75 \, n_{1,\text{kep}} \, J_2 \left(\frac{R_{\text{eq}}}{\mathbf{a}} \right)^2 (1 - 3 \cos^2 i) \qquad (3.14)$$

$$n_1 = n_{1,\text{kep}} + \Delta n + \omega \qquad (3.15)$$

$$T_N = \frac{2\pi}{n_1} \qquad (3.16)$$

3.2   Transformations

- **Geometry of the Sun Vector**
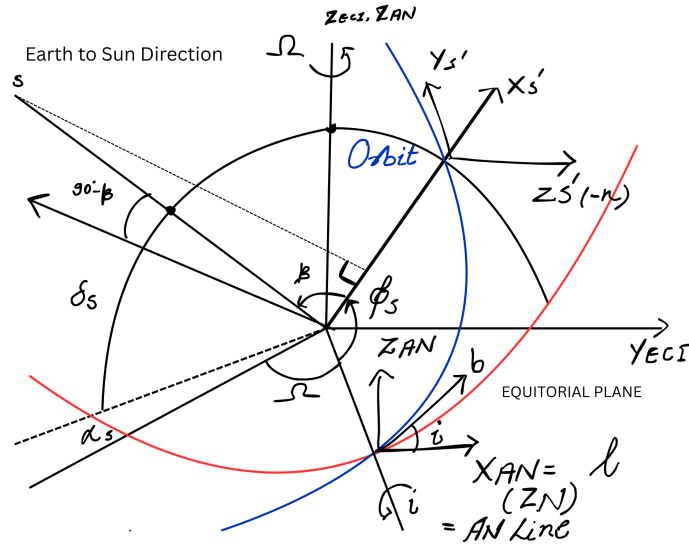
Figure 3.4: Geometry of the Sun Vector

Locate Sun relative to orbit plane

$\downarrow$

$(X_{ECI},\ Y_{ECI},\ Z_{ECI})$

$\downarrow$ (rotation about $Z_I = Z_{AN}, \Omega$)

$(X_{AN},\ Y_{AN},\ Z_{AN})$

$\downarrow$ (rotation about X_{AN}, i)

$(l,\ b,\ n)$ $\xrightarrow{\text{(rotation about } N, \phi_S)}$ $(X'_S,\ Y'_S,\ Z'_S)$

$\downarrow$ (rotation about N, ω) $(Z'_S = W = N)$

$(P,\ Q,\ W)$ $\downarrow$ (rotation about $Y'_S, -\beta$)

(Perifocal frame) (X_S, Y_S, Z_S) SUN

$\downarrow$ (rotation about $W, \phi_S - \omega$)

$(X'_S,\ Y'_S,\ Z'_S)$
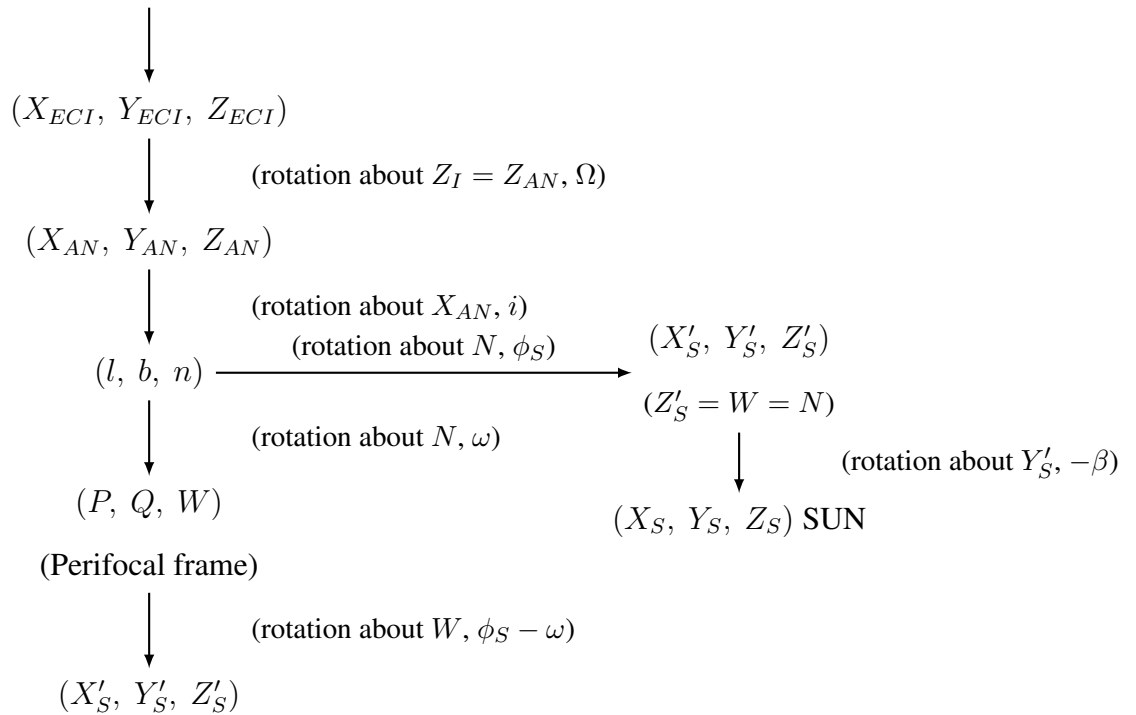
Derivation

It is known that the orbit normal **n** and the Earth-to-Sun vector are, in the ECI frame:

$$\mathbf{n} = \mathbf{W} = \begin{bmatrix} \sin i \sin \Omega \\ -\sin i \cos \Omega \\ \cos i \end{bmatrix}^{\mathcal{F}^I} \tag{3.17}$$

$$\mathbf{s} = \begin{bmatrix} \cos \delta_S \cos \alpha_S \\ \cos \delta_S \sin \alpha_S \\ \sin \delta_S \end{bmatrix}^{\mathcal{F}^I} \tag{3.18}$$

Then,

$$\mathbf{s} \cdot \mathbf{n} = \cos(90° - \beta) = \sin \beta = \sin i \sin \Omega \cos \delta_S \cos \alpha_S - \sin i \cos \Omega \cos \delta_S \sin \alpha_S + \cos i \sin \delta_S \tag{3.19}$$

or

$$\sin \beta = \sin i \cos \delta_S (\sin \Omega \cos \alpha_S - \cos \Omega \sin \alpha_S) + \cos i \sin \delta_S \tag{3.20}$$

$$\boxed{\sin \beta = \sin i \cos \delta_S \sin(\Omega - \alpha_S) + \cos i \sin \delta_S} \tag{3.21}$$

The Sun vector in the ECI frame is known to be:

$$\mathbf{u}_s^{\mathcal{F}^I} = \begin{bmatrix} c_{\delta_s} c_{\alpha_s} \\ c_{\delta_s} s_{\alpha_s} \\ s_{\delta_s} \end{bmatrix}^{\mathcal{F}^I} \tag{3.22}$$

Also

$$\mathbf{u}_s^{\mathcal{F}s} = \begin{bmatrix} 1 \\ 0 \\ 0 \end{bmatrix}^{\mathcal{F}s} \tag{3.23}$$

$$\mathbf{u}_s^{\mathcal{F}I} = R_z(-\Omega)R_x(-i)R_z(-\phi_s)R_y(\beta) \begin{bmatrix} 1 \\ 0 \\ 0 \end{bmatrix}^{\mathcal{F}s} \tag{3.24}$$

$$= \begin{bmatrix} cos_\Omega & -sin_\Omega & 0 \\ -sin_\Omega & cos_\Omega & 0 \\ 0 & 0 & 1 \end{bmatrix} \begin{bmatrix} 1 & 0 & 0 \\ 0 & cos_i & -sin_i \\ 0 & sin_i & cos_i \end{bmatrix} \begin{bmatrix} cos_{\phi_s} & -sin_{\phi_s} & 0 \\ sin_{\phi_s} & cos_{\phi_s} & 0 \\ 0 & 0 & 1 \end{bmatrix} \begin{bmatrix} cos_\beta \\ 0 \\ sin_\beta \end{bmatrix} \tag{3.25}$$

s in the ascending node frame:

$$\mathbf{s}^{\mathcal{F}I} = \begin{bmatrix} \cos\Omega & \sin\Omega & 0 \\ -\sin\Omega & \cos\Omega & 0 \\ 0 & 0 & 1 \end{bmatrix} \begin{bmatrix} cos_{\delta_s}cos_{\alpha_s} \\ cos_{\delta_s}sin_{\alpha_s} \\ sin_{\delta_s} \end{bmatrix}^{\mathcal{F}I} \tag{3.26}$$

$$= \begin{bmatrix} \cos\Omega\cos\delta_s\cos\alpha_s + \sin\Omega\cos\delta_s\sin\alpha_s \\ -\sin\Omega\cos\delta_s\cos\alpha_s + \cos\Omega\cos\delta_s\sin\alpha_s \\ \sin\delta_s \end{bmatrix} = \begin{bmatrix} \cos\delta_s\cos(\Omega - \alpha_s) \\ \cos\delta_s\sin(\alpha_s - \Omega) \\ \sin\delta_s \end{bmatrix} \tag{3.27}$$

$$\boxed{\alpha_A = \alpha_s - \Omega = \alpha_s \quad \text{from the Ascending Node}} \tag{3.28}$$

thus

$$\mathbf{s}^{\mathcal{F}^{AN}} = \begin{bmatrix} \cos \delta_s \cos \alpha_A \\ \cos \delta_s \sin \alpha_A \\ \sin \delta_s \end{bmatrix} \tag{3.29}$$

Now,

$$\mathbf{s}^{lbn} = R_x(i)\mathbf{s}^{\mathcal{F}^{AN}} \tag{3.30}$$

$$= \begin{bmatrix} 1 & 0 & 0 \\ 0 & \cos i & \sin i \\ 0 & -\sin i & \cos i \end{bmatrix} \begin{bmatrix} \cos \delta_s \cos \alpha_A \\ \cos \delta_s \sin \alpha_A \\ \sin \delta_s \end{bmatrix} = \begin{bmatrix} \cos \delta_s \cos \alpha_A \\ \cos i \cos \delta_s \sin \alpha_A + \sin i \sin \delta_s \\ -\sin i \cos \delta_s \sin \alpha_A + \cos i \sin \delta_s \end{bmatrix}^{lbn} \tag{3.31}$$

Thus:

$$\mathbf{s}^{lbn} = \begin{bmatrix} \cos \phi_s \cos \beta \\ \sin \phi_s \cos \beta \\ \sin \beta \end{bmatrix}^{lbn} \tag{3.32}$$

So, equate the l and b components and divide the b component with the l component:

$$\boxed{\tan \phi_s = \frac{\cos i \cos \delta_s \sin \alpha_A + \sin i \sin \delta_s}{\cos \delta_s \cos \alpha_A}} \tag{3.33}$$

- **Angles of Debris Location**
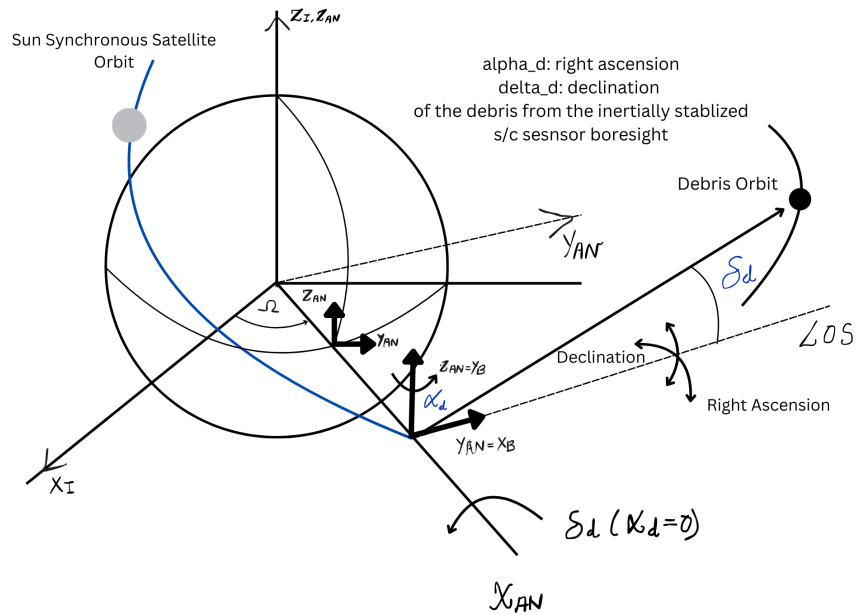
Figure 3.5: Angles of Debris Location

$$(X_I, \ Y_I, \ Z_I)$$

$$\downarrow \quad \text{(rotation about } Z_I = Z_{AN}, \Omega)$$

$$(X_{AN}, \ Y_{AN}, \ Z_{AN})$$

(U,E,N)

north, up, east

$$\downarrow$$

$$(X_b, \ Y_b, \ Z_b)$$

ascension α_d (right ascension)

$$\downarrow \quad \text{(rotation about } Z_b, \alpha_d)$$

$$\left(X'_b, \ Y'_b, \ Z'_b\right)$$

declination δ_d

$$\downarrow \quad \text{(rotation about } Y'_b, \delta_d)$$

$$(X_d, \ Y_d, \ Z_d)$$

debris
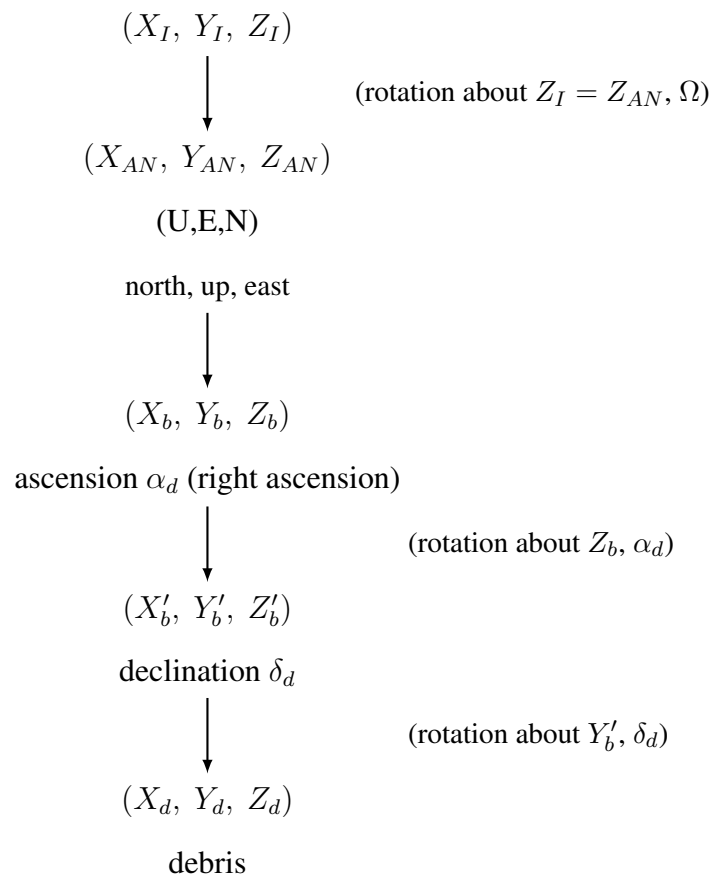
Derivation

$$u_\rho^{\mathcal{F}b} = R_y(-\alpha_d)R_z(-\delta_d)\begin{bmatrix} 1 \\ 0 \\ 0 \end{bmatrix} \tag{3.34}$$

$$\begin{bmatrix} X_b \\ Y_b \\ Z_b \end{bmatrix} = \begin{bmatrix} Y_{AN} \\ Z_{AN} \\ A_{AN} \end{bmatrix} = \begin{bmatrix} 0 & 1 & 0 \\ 0 & 0 & 1 \\ 1 & 0 & -0 \end{bmatrix} \begin{bmatrix} X_{AN} \\ Y_{AN} \\ Z_{AN} \end{bmatrix} [8] \tag{3.35}$$

Expanding step-by-step:

$$= R_y(-\alpha_d)\begin{bmatrix} \cos\delta_d & -sin\delta_d & 0 \\ \sin\delta_d & cos\delta_d & 0 \\ 0 & 0 & 1 \end{bmatrix}\begin{bmatrix} 1 \\ 0 \\ 0 \end{bmatrix} \tag{3.36}$$

$$= \begin{bmatrix} \cos\alpha_d & 0 & \sin\alpha_d \\ 0 & 1 & 0 \\ -\sin\alpha_d & 0 & \cos\alpha_d \end{bmatrix}\begin{bmatrix} \cos\delta_d \\ -\sin\delta_d \\ 0 \end{bmatrix} \tag{3.37}$$

Thus:

$$= \begin{bmatrix} \cos\alpha_d\cos\delta_d + \sin\alpha_d \times 0 \\ -\sin\delta_d \\ -\sin\alpha_d\cos\delta_d + \cos\alpha_d \times 0 \end{bmatrix} = \begin{bmatrix} \cos\alpha_d\cos\delta_d \\ -\sin\delta_d \\ -\sin\alpha_d\cos\delta_d \end{bmatrix} \tag{3.38}$$

And writing debris along X_b':

$$\begin{bmatrix} u_{\rho X_b} \\ u_{\rho Y_b} \\ u_{\rho Z_b} \end{bmatrix} = \begin{bmatrix} \cos \alpha_d \cos \delta_d \\ \sin \delta_d \\ -\sin \alpha_d \cos \delta_d \end{bmatrix} \tag{3.39}$$

$$\delta_d = \sin^{-1}(u_{\rho Y_b}) \tag{3.40}$$

$$\delta_d = \sin^{-1}(u_{\rho Z_A}) \tag{3.41}$$

From the components:

$$\sin \alpha_d \cos \delta_d = -u_{\rho Z_b} \tag{3.42}$$

$$\cos \alpha_d \cos \delta_d = u_{\rho X_b} \tag{3.43}$$

Thus:

$$\tan \alpha_d = \frac{-u_{\rho Z_b}}{u_{\rho X_b}} = \frac{-u_{\rho X_A}}{u_{\rho Y_A}} \tag{3.44}$$

Also, solving for $\cos \delta_d$:

$$\cos \delta_d = \sqrt{u_{\rho X_b}^2 + u_{\rho Z_b}^2} \quad \text{(positive by definition of } \delta_d\text{)} \tag{3.45}$$

$$\tan \delta_d = \frac{u_{\rho Y_b}}{\sqrt{u_{\rho X_b}^2 + u_{\rho Z_b}^2}} = \frac{u_{\rho Z_A}}{\sqrt{u_{\rho Y_A}^2 + u_{\rho X_A}^2}} \tag{3.46}$$

Finally, for the angle:

$$\tan \alpha_d = \frac{-u_{\rho Z_b}}{u_{\rho X_b}} = \frac{-u_{\rho X_b}}{u_{\rho Y_b}} \tag{3.47}$$

• **Visibility of Debris above Horizon**
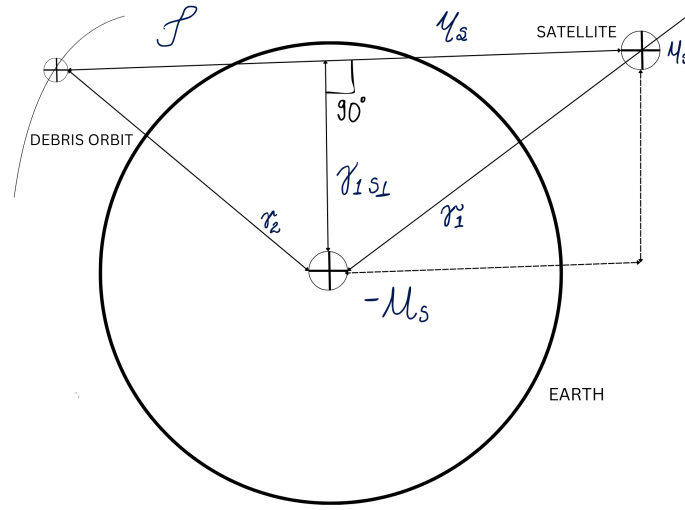
Figure 3.6: Visibility of Debris above Horizon

$$\vec{\rho} = \vec{r}_2 - \vec{r}_1 \quad \text{and} \quad \vec{u}_\rho = \frac{\vec{\rho}}{|\vec{\rho}|} \tag{3.48}$$

Component of $\vec{r}_1$ along $\vec{\rho}$:

$$(\vec{r}_1 \cdot (-\vec{u}_\rho))\vec{u}_\rho \quad \text{or along} \quad (\vec{r}_1 \cdot (-\vec{u}_\rho))(-\vec{u}_\rho) \tag{3.49}$$

Thus:

$$\vec{r}_{1\perp} + (\vec{r}_1 \cdot (-\vec{u}_\rho)) - \vec{u}_\rho = \vec{r}_1 \quad \Rightarrow \quad \vec{r}_{1\perp} = \vec{r}_1 + (\vec{r}_1 \cdot (\vec{u}_\rho))\,\vec{u}_\rho \tag{3.50}$$

or equivalently:

$$\vec{r}_{1\perp} = \vec{r}_1 - (\vec{r}_1 \cdot \vec{u}_\rho)\vec{u}_\rho \tag{3.51}$$

$$\vec{r}_{1\perp} = \vec{r}_1 + \vec{r}_1 \cdot (-\vec{u}_\rho)\vec{u}_\rho \tag{3.52}$$

Then, for conditions:

$$|\vec{r}_{1\perp}| > R_{\text{eq}}\text{Visible} \quad \text{and} \quad |\vec{r}_{1\perp}| < R_{\text{eq}} \text{ Not Visible hitting the Earth} \tag{3.53}$$

- **Tracking the Debris** A diagram showing the position vector $\vec{\rho}$ from a satellite to debris with unit direction vector $\vec{u}_\rho$, angular velocity $\vec{\omega}_\rho$, and rate of change $\dot{\vec{\rho}}$.
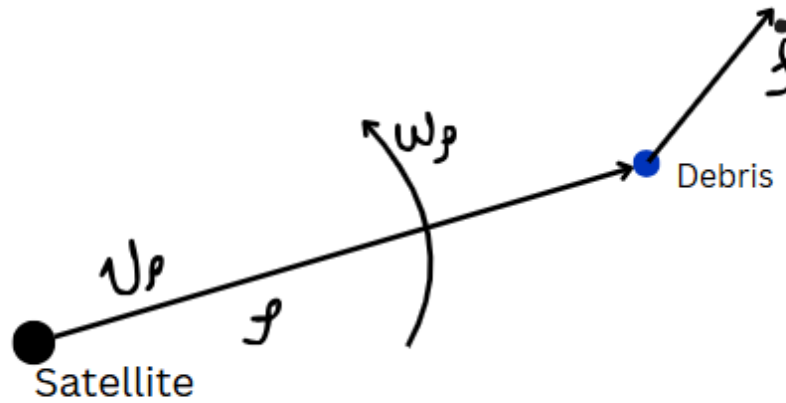
Figure 3.7: Inertial angular rates of debris

Note:

$2 = $ debris, $\quad 1 = $ the satellite with the optics

$$\vec{\rho} = \vec{r}_2 - \vec{r}_1 \tag{3.54}$$

$$\dot{\vec{\rho}} = \dot{\vec{r}}_2 - \dot{\vec{r}}_1 \tag{3.55}$$

$$\vec{\rho} = \rho\,\vec{u}_\rho \tag{3.56}$$

Inertial:

$$\dot{\vec{\rho}} = \rho\,\dot{\vec{u}}_\rho + \dot{\rho}\,\vec{u}_\rho \tag{3.57}$$

$$= \rho\,\vec{\omega}_\rho \times \vec{u}_\rho + \dot{\rho}\,\vec{u}_\rho \tag{3.58}$$

$$\vec{\omega}_\rho = \frac{\vec{\rho}}{\rho^2} \times \dot{\vec{\rho}} = \frac{1}{\rho} \vec{u}_\rho \times \dot{\vec{\rho}} \tag{3.59}$$

Inertial Angular Rates of the Debris in body frame:

$$\vec{\omega}_d^b = \dot{\alpha}_d \, \hat{j}_b + \dot{\delta}_d \, \hat{k}_b \tag{3.60}$$

Transformation matrix:

$$\begin{bmatrix} \dot{\delta}_d \, \sin \alpha_d \\ \dot{\alpha}_d \\ \dot{\delta}_d \, \cos \alpha_d \end{bmatrix}^b = \vec{\omega}_d^b \tag{3.61}$$

$$\dot{\alpha}_d = \frac{1}{\rho} \left(\vec{u}_{zb} \times \dot{\vec{\rho}} - \vec{u}_{xb} \times \dot{\vec{\rho}} \right) \tag{3.62}$$

$$\dot{\delta}_d = \frac{1}{\rho \cos \alpha_d} \left(-\vec{u}_{yb} \cdot \dot{\vec{\rho}} + \vec{u}_{xb} \cdot \dot{\vec{\rho}} \right) \tag{3.63}$$

3.3 Payload

Star Tracker A star tracker is an optical device designed to observe the space environment by detecting stars and determining the orientation of a spacecraft based on their positions. Using a sensitive camera with a wide field of view, the star tracker captures images of stars against the dark background of space. These observed stars are then identified by comparing their positions and brightness to a preloaded star catalog, which contains detailed spatial coordinates of known stars. Once identified, the star tracker calculates the spacecraft's orientation by determining the angular position and direction of the stars relative to the spacecraft's reference frame.

While its primary purpose is to aid in spacecraft attitude determination, the star tracker can

also observe the space environment by detecting anomalies in the star field, such as moving objects that may indicate the presence of space debris. These objects are distinguished from stars by their motion or unexpected patterns in the data. The information collected by the star tracker is integrated into the spacecraft's navigation and control systems, ensuring precise alignment for mission objectives such as pointing scientific instruments or aligning solar panels.
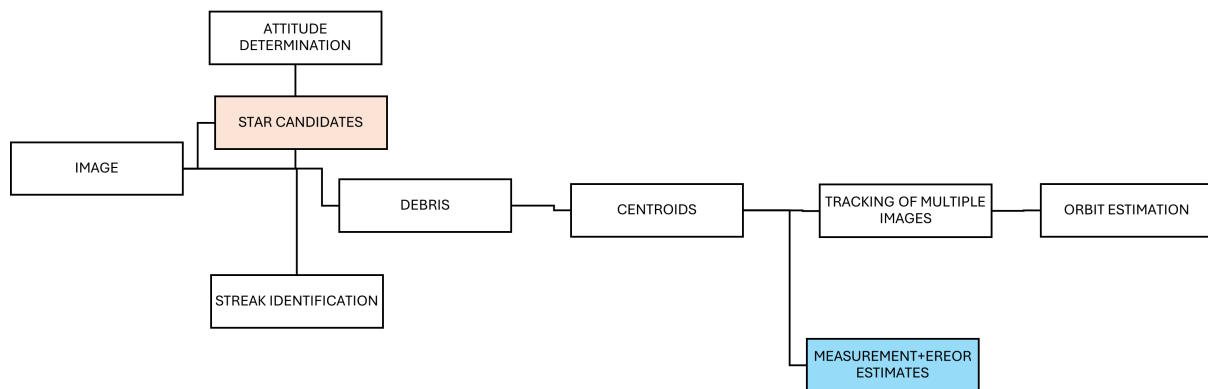
Figure 3.8: Workflow of Star Tracker

Chapter 4

Results

4.1 Force Model Analysis

- **J2 Effect** Simulation of a Satellite under the effects of J2. The satellite was simulated in an orbit of 450 km radially away from Earth. The simulation shows the change in true anomaly, right ascension, inclination angle, semi-major axis, argument of perigee, angular acceleration and J2 gravitational acceleration in 2 orbit rotations. It takes about 93.6 minutes for a satellite in such orbit to complete a revolution around Earth.
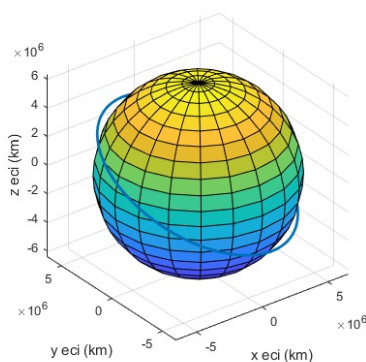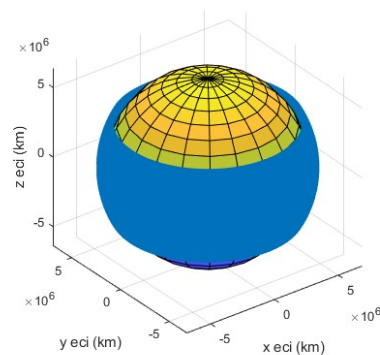
(a) 2 orbit Revolutions	(b) 2804 orbit Revolution (6 months)

Figure 4.1: Orbit Simulation

The orbit simulation for above parameters is done for 6 months, but to understand the precession the 2 orbit simulation are assessed.
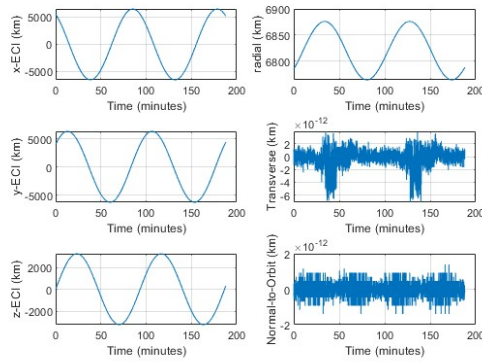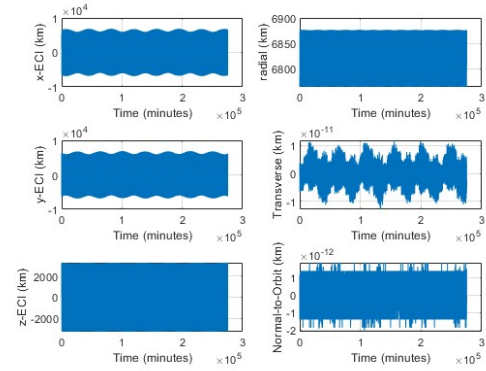
(a) 2 orbit Revolutions   (b) 2804 orbit Revolution (6 months)

Figure 4.2: Movement in X,Y,Z and Radial Directions

The above figure explains that in 2 orbit movement there is about 100 km change in all directions.
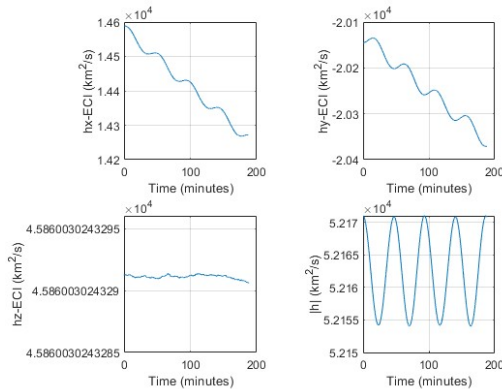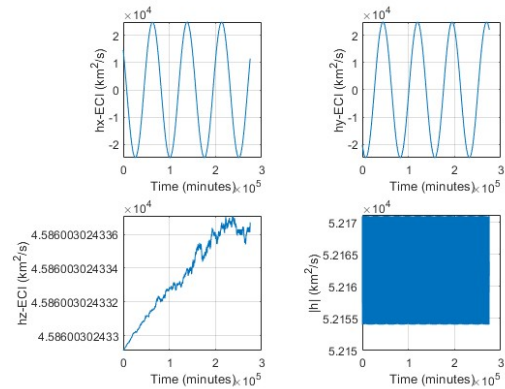
(a) 2 orbit Revolutions   (b) 2804 orbit Revolution (6 months)

Figure 4.3: Angular Momentum

For 2 orbit simulation the angular momentum change in all the 3 directions and absolute change in angular momentum is observed, the angular momentum in x-direction decreased from 1.46×10^4 km^2/s to 1.42×10^4 km^2/s. It decreases to -2.01×10^4 km^2/s to -2.04×10^4 km^2/s in y-direction. In z-direction it remains constant. In absolute terms it oscillates.
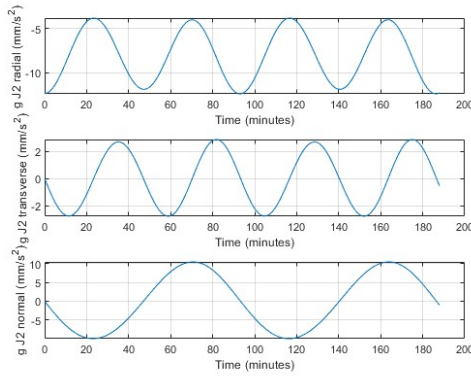
(a) 2 orbit Revolutions
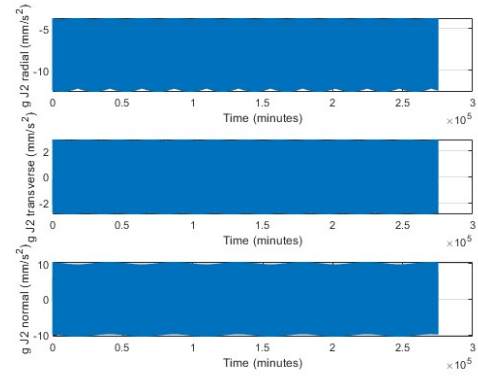
(b) 2804 orbit Revolution (6 months)

Figure 4.4: Gravitation Acceleration J2

In 2 orbit revolutions, the gravitational acceleration in the Radial direction oscillates between 0 and 5 mm per second square, in the Traverse direction it oscillates between -2 and 2 mm per second square, and in the Normal direction it oscillates between -10 and 10 mm per second square. Over time, these oscillations add up and cause a bigger change.
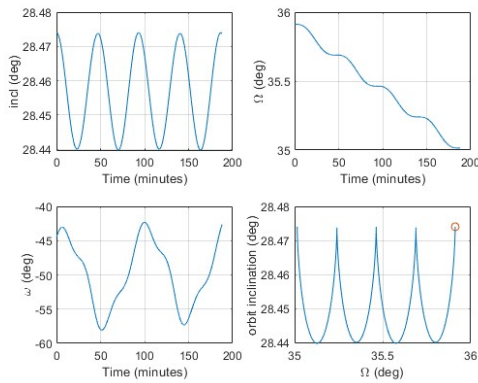
(a) 2 orbit Revolutions
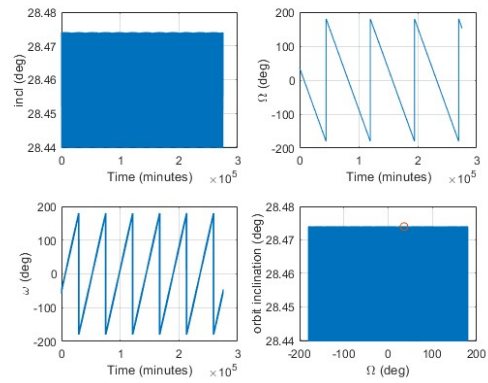
(b) 2804 orbit Revolution (6 months)

Figure 4.5: Inclination Angle, Argument of Perigee, Right Ascension Angle and Orbit Inclination vs Right Ascension

In 2 orbit revolutions we observe that the inclination angle oscillates between 28.485 degrees to 28.44 degrees, the right ascension angle decreases to about 1 degree but in 6 months duration it oscillates between -197 degrees to 197 degrees. The argument of perigee oscillates between -47 degrees to -58 degrees.
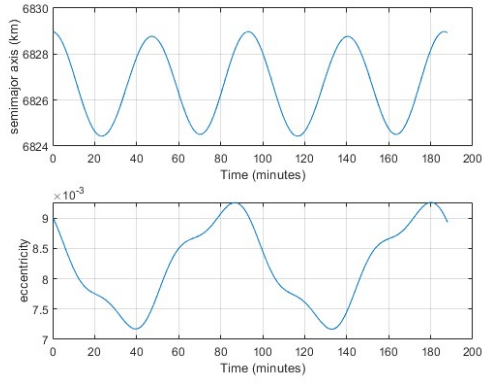
(a) 2 orbit Revolutions
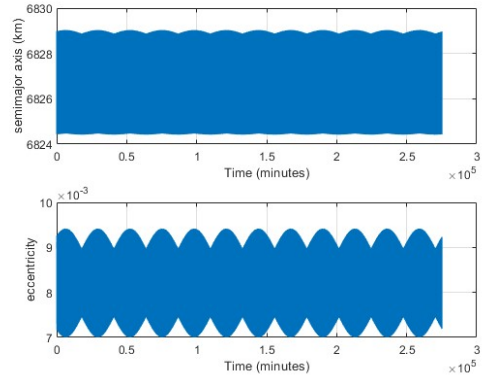
(b) 2804 orbit Revolution (6 months)

Figure 4.6: Inclination Angle, Argument of Perigee, Right Ascension Angle and Orbit Inclination vs Right Ascension

The semi major axis also oscillates between 6829 kms to 6825 kms, the eccentricity also oscillates between 9×10^{-3} to 7.1×10^{-3}. The similar trend will continue for 6 months between the same values.
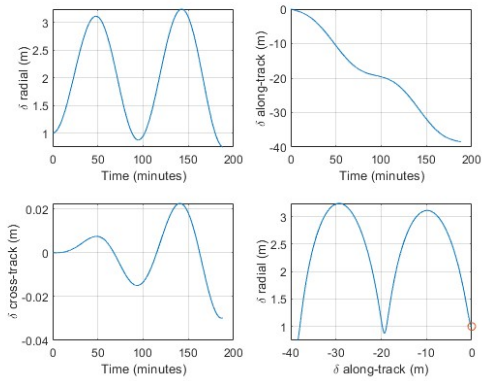
(a) 2 orbit Revolutions
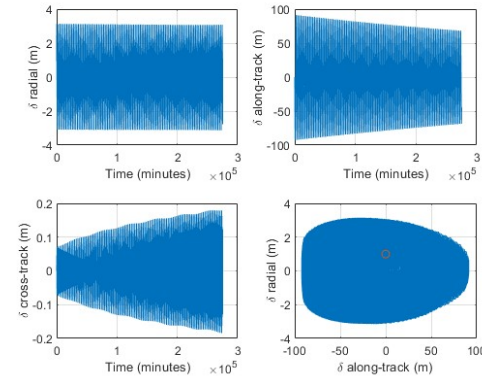
(b) 2804 orbit Revolution (6 months)

Figure 4.7: The difference between Spherical Earth and Non Spherical Earth (J2)

In 2 orbit revolutions we observe the oscillations along radial and cross Track direction but along the track there is a decay for 40 m. These are cumulative changes showing up which were seen in form of change in angular momentum and acceleration due to gravity.

Hence the study conclusively shows J2 effects are prominent and are important to account for during a mission planning.

The other effects such as aerodynamic drag, relativistic effects, earth tides, earth radiation pressure, solar radiation pressure are not so prominent in the LEO environment. [6]

4.2   Satellite Orbit

- **Satellite in J2 Orbit-Sun synchronous** The host satellite orbit is a sun-synchronous, dawn-dusk satellite, with semi-major axis at 7098.137 km, eccentricity 0, inclination angle 98.3 degrees, true anomaly 0 degrees, and right ascension 90 degrees. The section discusses the precession of different orbital factors. The orbital period is 99.19 minutes. The satellite precesses from 1021 km to -1021 km in X_{ECI} axis, from 7092 km to -7092 km in Y_{ECI} axis and 7017 km to -7017 km in Z_{ECI} axis.
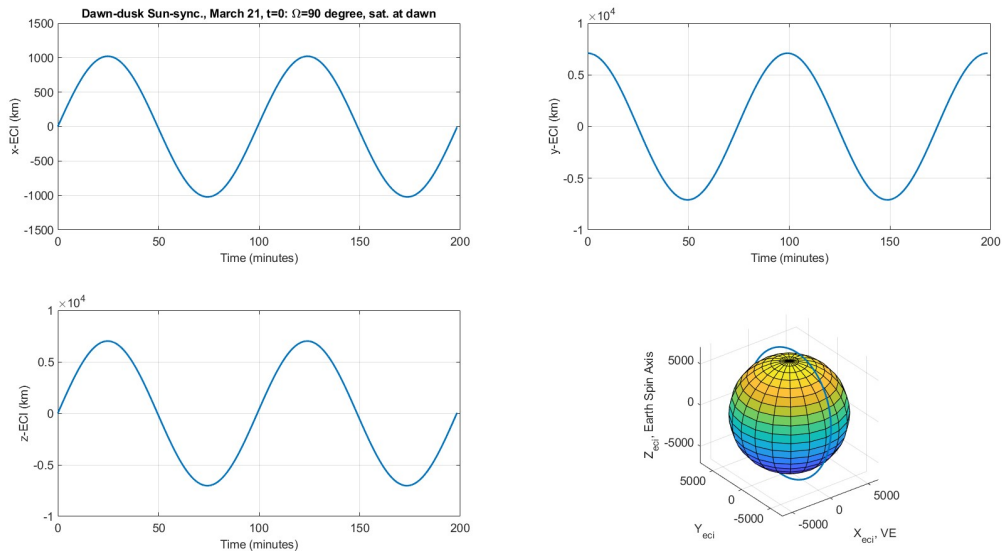
Figure 4.8: Satellite Movement along X-eci,Y-eci,Z-eci

The angular momentum under J2 effect is not conserved. The angular momentum vector precesses under the effect. The left plot shows the limits of the angular momentum in the simulation time, though the angular momentum changes from 0,0,0 m^2/s in X,Y and Z direction to 56638.4 m^2/s, 2.109 $\times 10^{-7}$ m^2/sin Y and -7647.87 m^2/s in Z direction. However the precession in the Y direction is far smaller as compared to the one in the Z direction the right plot shows the precession of tip of the angular momentum vector.
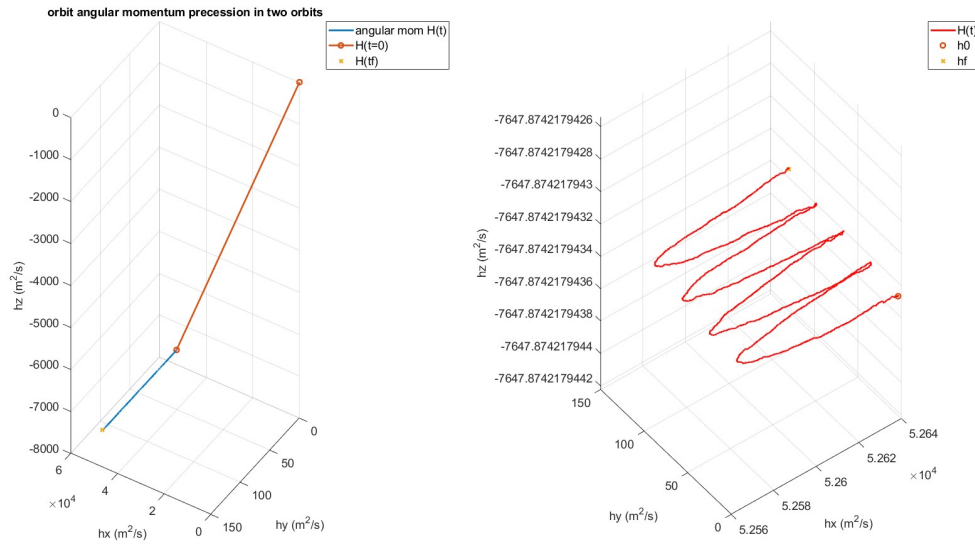
Figure 4.9: Angular Momentum Vector

The debris orbit is an ecliptic orbit with semi-major axis at 12000 kms, eccentricity 0.3, inclination angle 0 degrees, argument of perigee 60 degrees, true anomaly as 80 degrees and right ascension angle as 40 degrees. Under J2 effects there is wave like movement of the debris along X,Y and Z axis. The orbit period is 218 minutes.
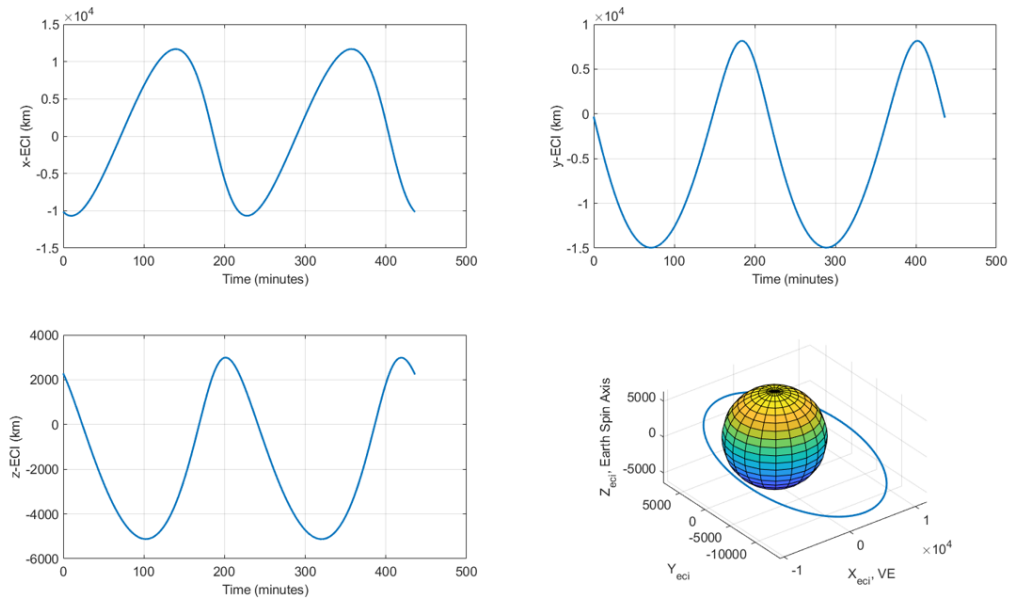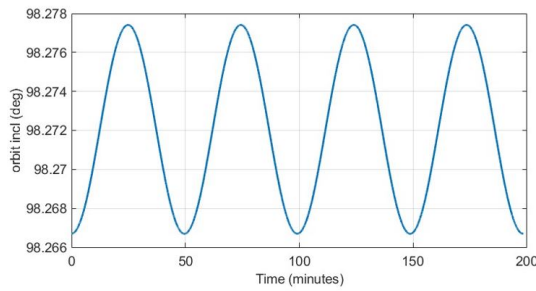

Figure 4.10: Debris Movement along X-eci,Y-eci,Z-eci

The semi-major axis varies from 7098 km to 7079 km. The eccentricity precesses from 0 to 1.7×10^{-3} in 200 mins. The orbit inclination varies from 98.267 degrees to 98.277 degrees, the right ascending node angle varies from 90 degrees to 90.13 degrees.
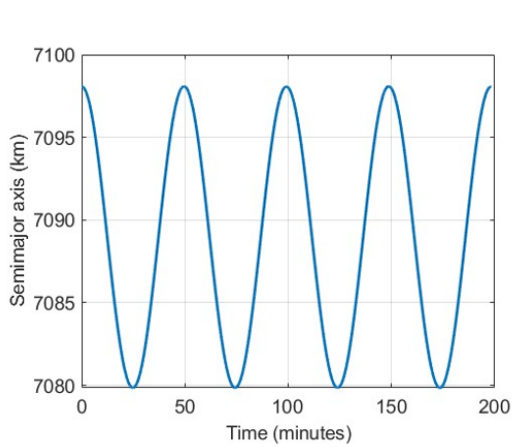
(a) Semi-major axis vs Time
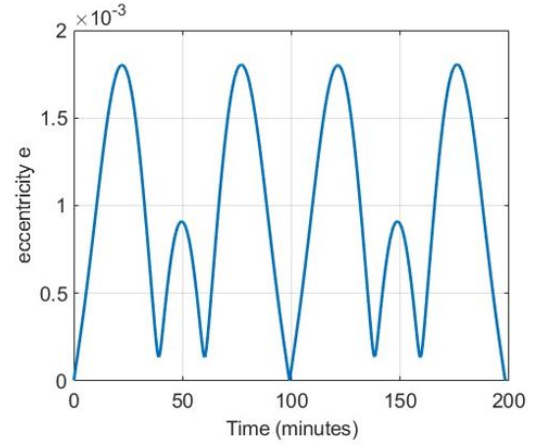
(b) Eccentricity vs Time

(c) Orbit inclination vs Time
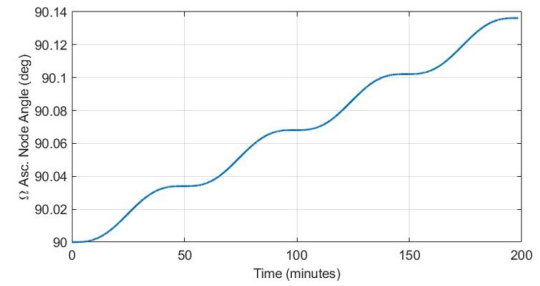
(d) Right ascension angle vs time
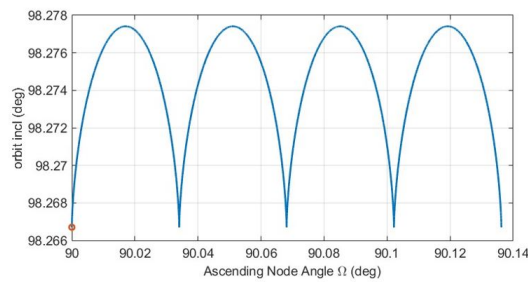
(e) Inclination vs Right ascension angle

Orbital parameters

The acceleration due to gravity vector precesses from 5.83 mm/s^2 to -5.83 mm/s^2 in x-direction, -10.2303mm/s^2 to 13.90 mm/s^2 and then to -13.91 mm/s^2 in y-direction and -0.39 mm/s^2 to -9.27 mm/s^2 to 19.47 mm/s^2 to -9.27 mm/s^2 and to -19.52 mm/s^2 in

z-direction.
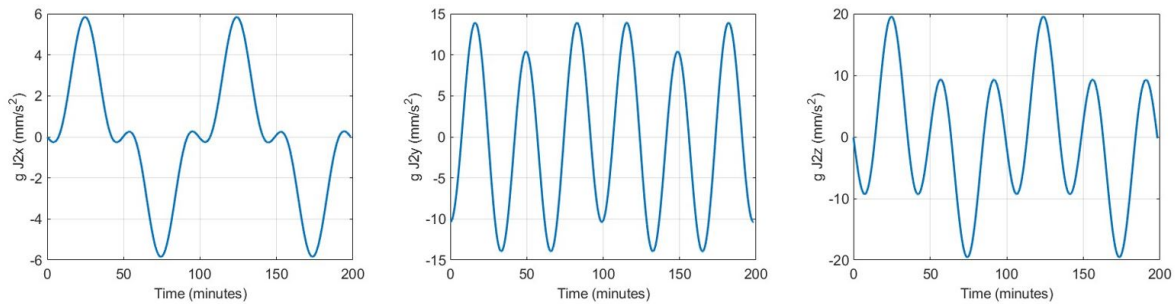
Figure 4.12: Acceleration due to gravity

4.3 Test Debris Orbit

- **Debris Orbit under J2 Effect**

  The angular momentum is conserved in a system where no external forces are available. But as we account for J2 effect, the momentum is not conserved. In the orbit the angular momentum vector momentum also precesses. The left plot shows the limits of angular momentum in the simulation time, the angular momentum changes from 0 m^2/s to 6.1996 m^2/s, however the magnitude of vector h drawn from the origin is much greater, hence it doesn't seem to be precessing. The angular momentum precession of the tip of the vector could be observed in the right plot. The plot shows how the vector traverses from the hx 1.444 m^2/s, hy -1.7325 m^2/s and hz 6.1996335998644 m^2/s to hx 1.4485 m^2/s, hy -1.7325 m^2/s and hz 6.1996335998654 m^2/s.
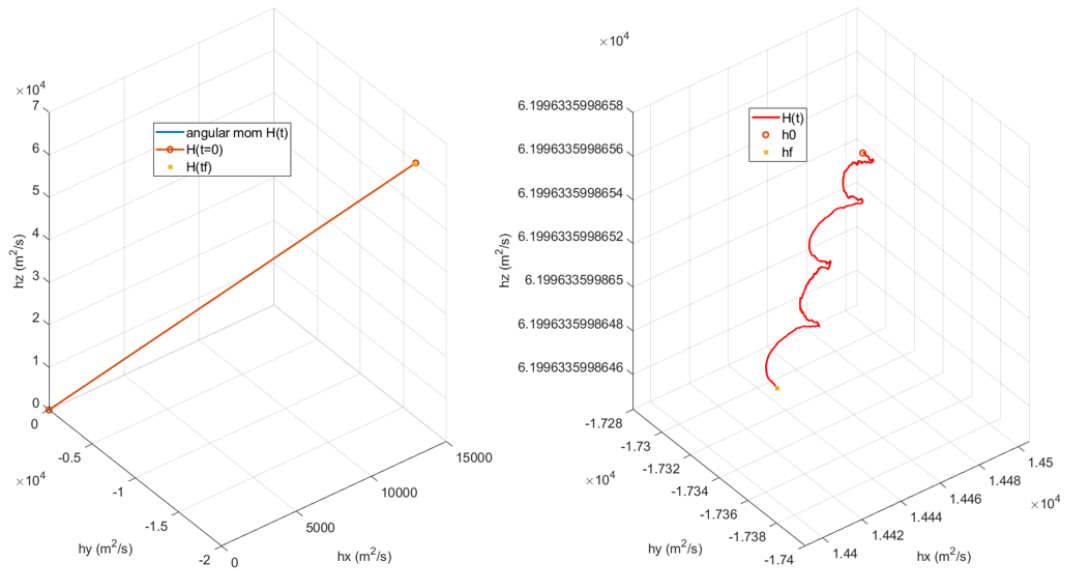
Figure 4.13: Angular Momentum Vector

The acceleration due to gravity vector precesses from 1.5 mm^2/s to -1.5 mm^2/s in x-direction, 0.2 mm^2/s to -3.8 mm^2/s in y-direction and -1.2 mm^2/s to -4.2 mm^2/s in z direction.
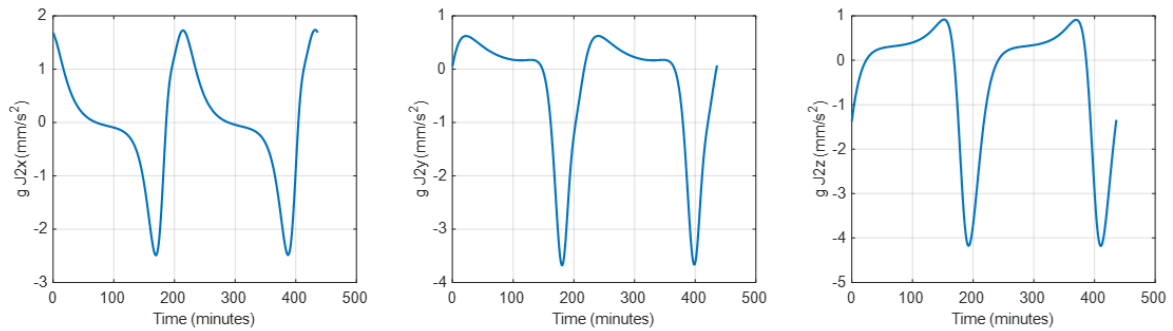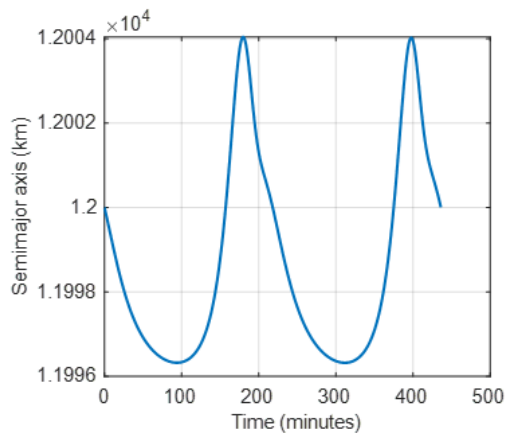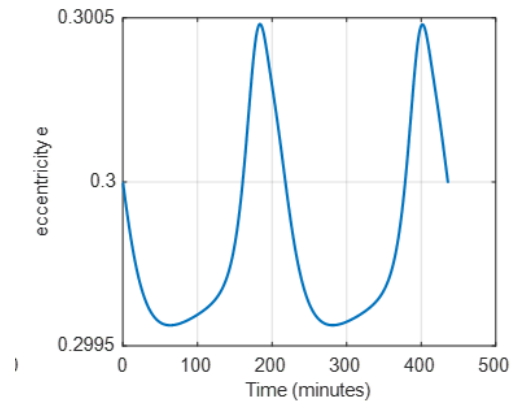

Figure 4.14: Acceleration due to gravity

The semi-major axis varies from 12000 km to 12004 km in the 435 minutes i.e 2 orbits, The eccentricity precesses from 0.3 to 0.3005 in 435 minutes. The orbit inclination varies from 20 degrees to 20.005 degrees, the right ascending node angle varies from 40 degrees

to 39.72 degrees.

(a) Semi-major axis vs Time
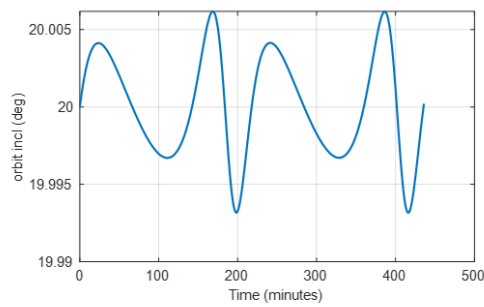
(b) Eccentricity vs Time)

(c) Orbit inclination vs Time
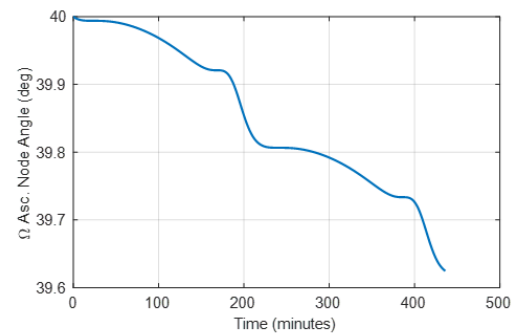
(d) Right ascension angle vs time
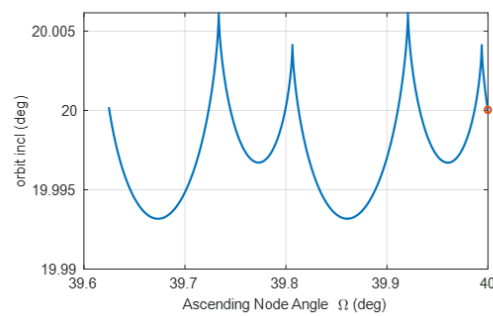
(e) Inclination vs Right ascension angle

Figure 4.15: Orbital parameters

The other effects such as aerodynamic drag, relativistic effects, earth tides, earth radiation pressure, solar radiation pressure are not so prominent at 12000 km [6].

4.4   Sun Angles

The sun ascension angle developed from the above equations, the α_s and δ_s are expressed in the equatorial plane where as ν is expressed in the ecliptic plane, the plots below shows the difference between the ascension angles and declination in both the planes, the plots attempt to signify the validation of math developed i.e. the pointing towards the sun in the course of 720 days.
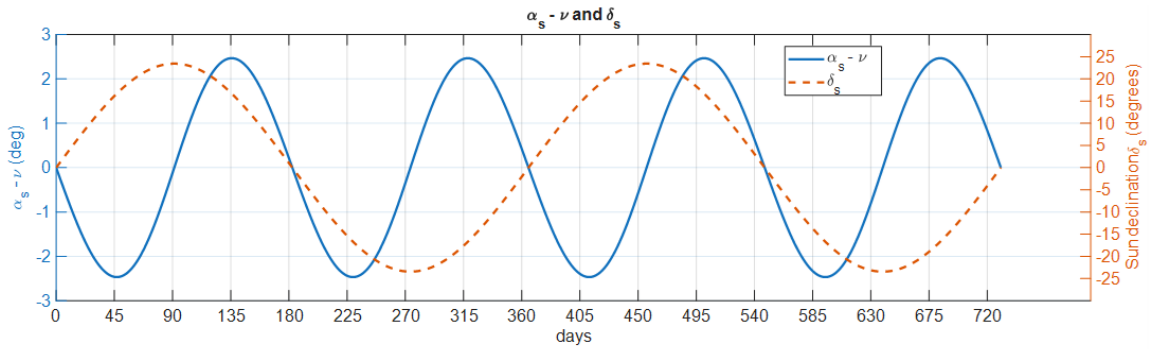

Figure 4.16: Difference between Sun angles in ecliptic plane and the equatorial plane and Sun pointing along the X_{sun} axis
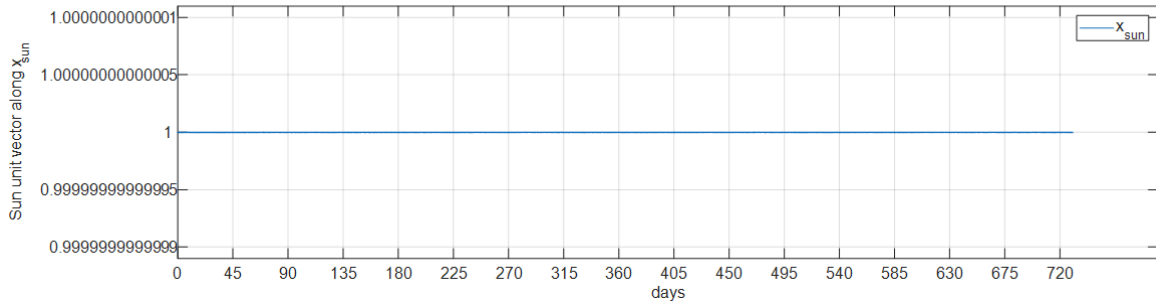

Figure 4.17: Sun vector pointing along X_{sun}

In the dawn dusk orbit the ascending node angle Ω and sun ascension angle α_s maintains 90 degree difference throughout. The β angle expressed in the orbit plane also known as sun angle and the declination angle δ_s, the phase angle ϕ_s projection of sun vector angle and the Sun angle from the ascending node α_s are also plotted. These plots helps in accounting the radiance from the sun, thus helping in how the debris will be illuminated by the sun.
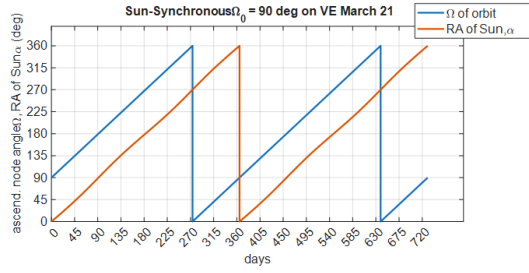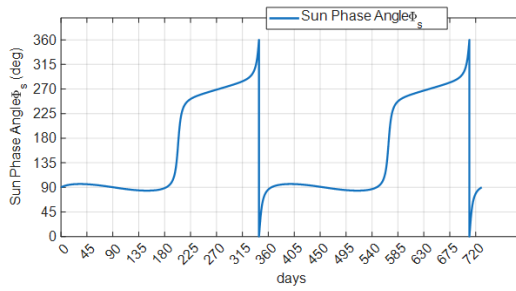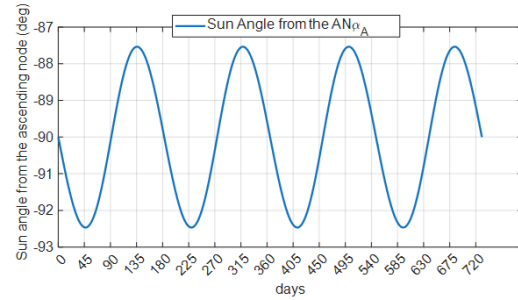
(a) Ascending node angle and Right ascension Sun
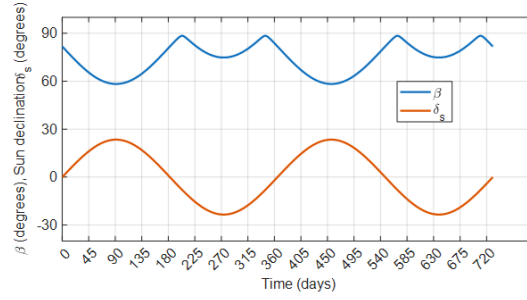
(b) Sun angle β and Declination angle δ_s

(c) Sun phase angle ϕ_s

(d) Sun angle from ascending node

4.5 Imaging Satellite and Debris

After observing the satellite at different altitudes like 450 km and 720 km, due to operational requirements, the satellite will be placed at an altitude of 720 km, i= 97 degrees and the other parameters discussed in the Section 3.1. In this section the sidereal tracking is discussed. The motion of satellite and debris in the ECI frame is depicted below.
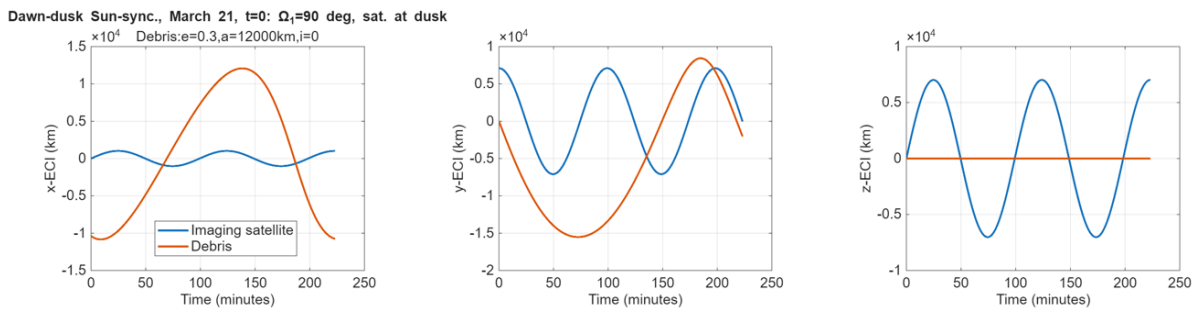

Figure 4.19: Motion of Satellite and Debris in ECI frame

The visibility of the debris with respect to the range is discussed. Range here is the vector from the satellite to the debris 3.6.
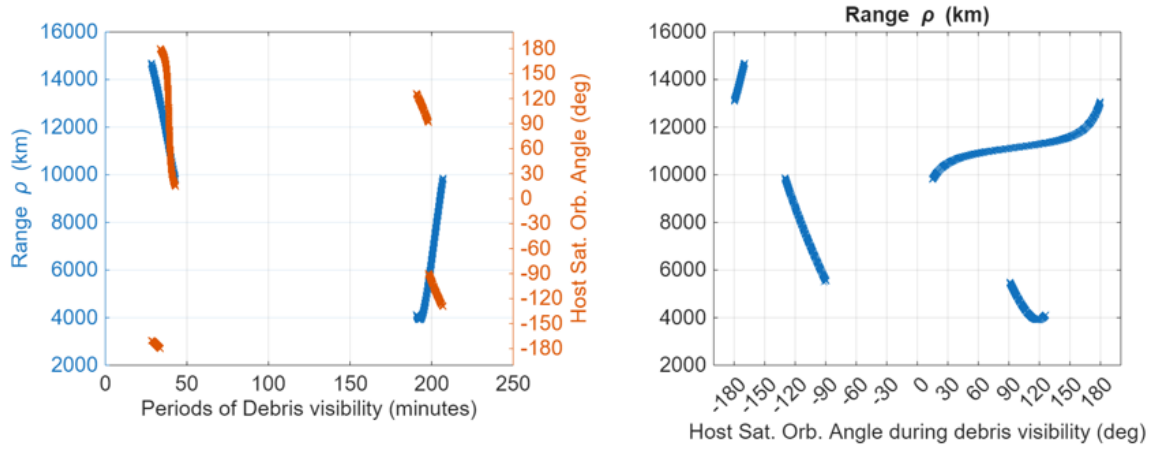

Figure 4.20: Range ρ vs Host satellite orbit angle

The derbis motion in the frontal hemisphere of the host satellite are discussed below: The perpendicular component of r1 i.e. a radial component extended to the range ρ, as discussed in the visibility of derbis above horizon, will depict the conditions of visibility of debris to the satellite i.e. $r_{1\perp}$ should be greater than R_{eq}.
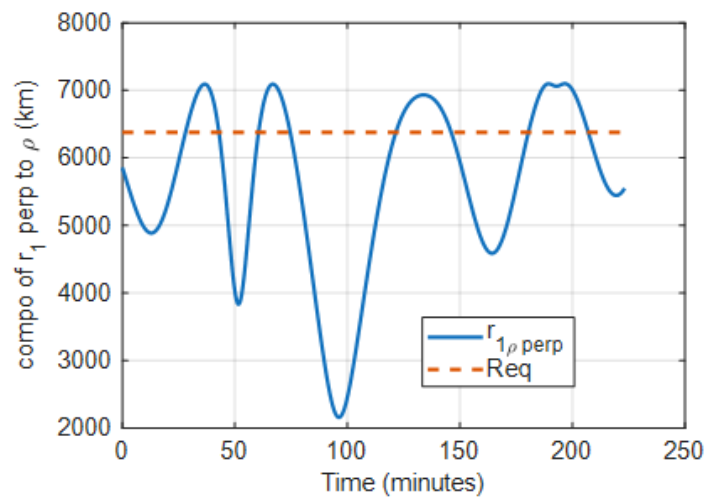

Figure 4.21: Condition for debris visibility

Due to the limited focal plane space that is 7×7 degrees, the debris angle that streaks across the focal plane is also limited. The following chart depicts how the debris streaks in the corresponding range; the camera focal plane is inertially stabilized. The α_d has the range of -45 degrees to +45 degrees, as beyond these limits the either the focal plane would hit the earth or it would start pointing towards the sun which will damage the sensor[9].
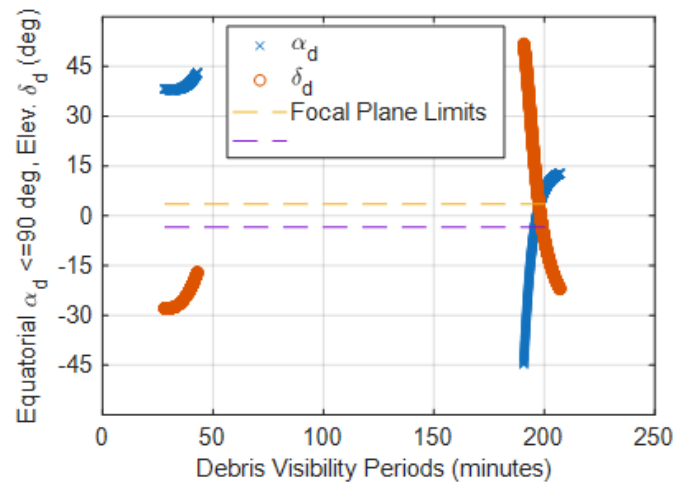

Figure 4.22: Debris visibility in the focal plane limits

The plots show how the debris will enter the focal plane and the debris streak in the focal plane.

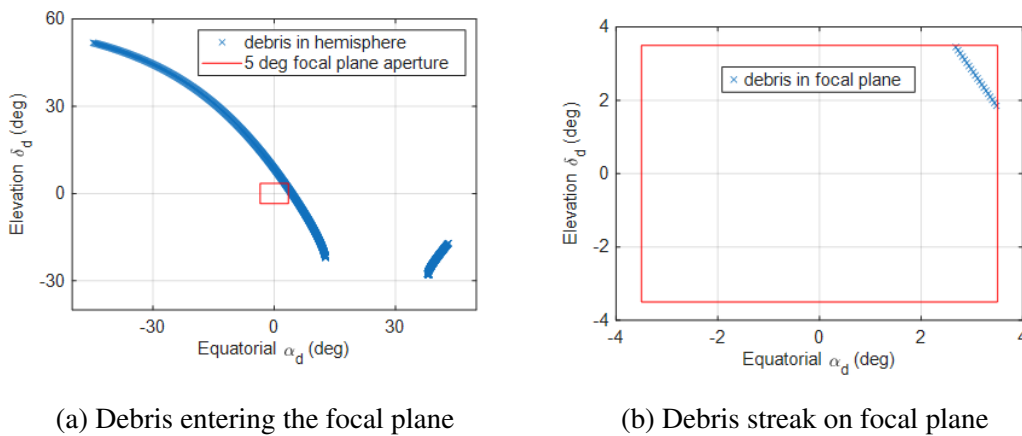(a) Debris entering the focal plane

(b) Debris streak on focal plane

Figure 4.23: Debris streak on focal plane

The debris is visible for 20 seconds on the focal plane, and the debris is in a range of 5200

km to 5350 km.

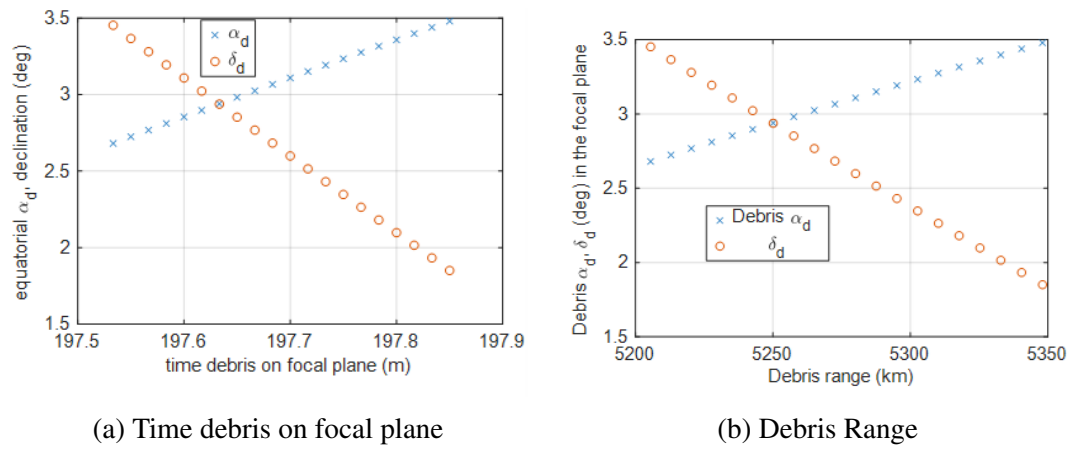(a) Time debris on focal plane   (b) Debris Range

Figure 4.24: Debris time and range on focal plane

For tracking an entity, the relative velocity of the debris becomes crucial; the plot depicts the relative velocity of debris and satellite against the range rate, i.e., how fast the image is traversing on the focal plane.
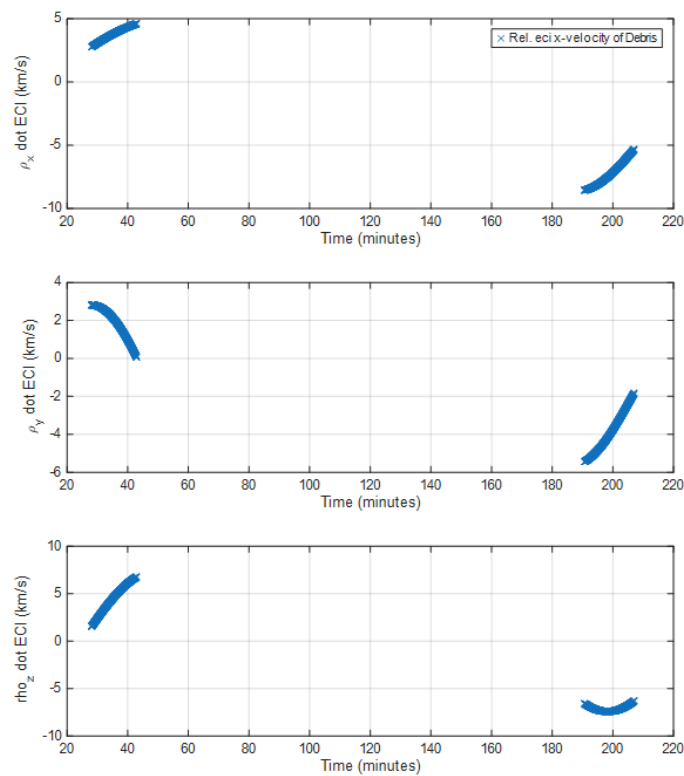

Figure 4.25: Range rate vs relative velocity

Measurements of the equatorial angular rate (α_d) and declination angular rate (δ_d) of debris during visibility periods are instrumental in designing a gimbaled camera station. These measurements enable the system to adjust its orientation dynamically, maintaining the debris within the camera's focal plane for extended durations, thereby improving tracking accuracy and observation quality [9].
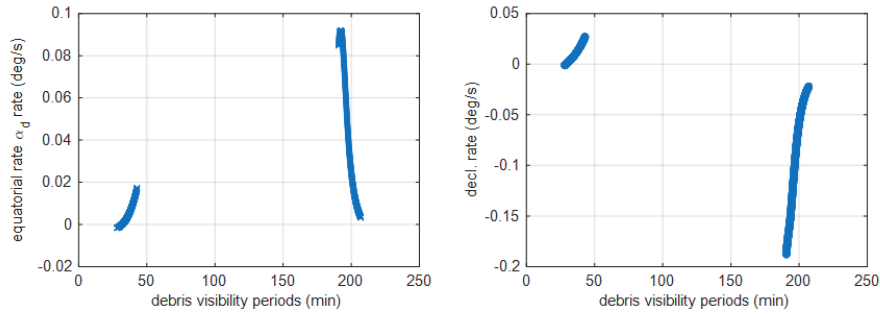
(a) Debris equator angle and declination angle
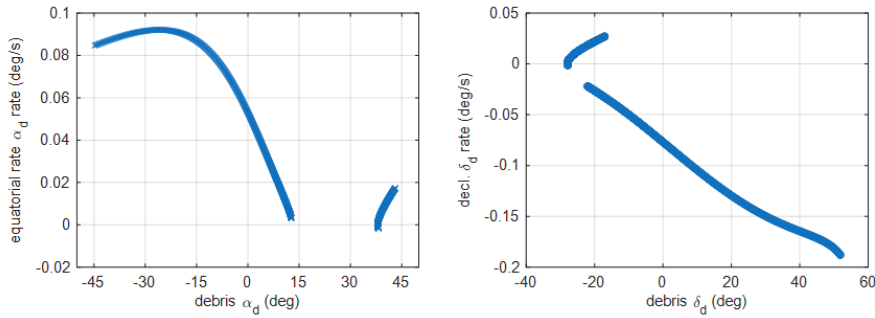
(b) Debris Equator angle rates and declination angle rates
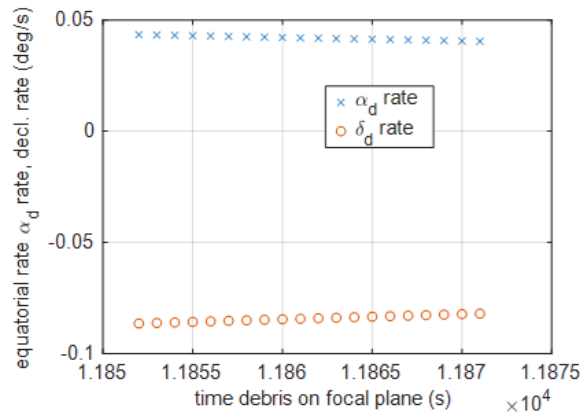
(c) Debris Equator angle rates and declination angle rates vs time

Figure 4.26: Debris Equator angle (-45 to +45 degrees) and declination angle and their rates relative to the inertially-stabilized visible-optic sensor

Chapter 5

Future Work

A PID controller for ephemeris tracking of the sky. In future work, the development of a robust PID (Proportional-Integral-Derivative) controller will leverage inputs from star tracker to achieve precise spacecraft attitude control. The star tracker will serve as the primary source of orientation data by identifying and tracking stars to determine the spacecraft's attitude. Integrating these systems will establish a feedback loop for the PID controller, facilitating accurate and responsive adjustments to the spacecraft's orientation. The relative debris angles in the focal plane are mapped to the inertial right ascension and declination angles using the sensor attitude estimate and the satellite inertial position, estimated onboard autonomously with GPS and NavIC signals, using the GRAPHIC (Group and Phase Ionospheric Correction) and integer ambiguity resolution for high accuracy (3m, 1-sigma). The equilibrium temperature of the debris in space will be determined, and its radiance compared with the noise energy of the space background. A suitable signal-to-noise ratio will be used to detect the debris in the myriad space objects in the focal plane. We will explore ephemeris tracking, in which the sensor tracks the debris to gather sufficient measurements [4]. For scanning the equatorial celestial region the sensor will perform step and stare scans in right ascension and declination[10]. The Laplace and Goodings Techniques will be used for initial orbit determination of the debris, the accuracy of which will be governed by the focal plane measurement errors compounded with the satellite orbit and attitude estimation errors.

Bibliography

[1] California Polytechnic State University. CalPoly-CDS-Rev.13, CubeSat Design Specification. CubeSat Design Specification Rev.13, California Polytechnic State University, San Luis Obispo, 2014.

[2] Camille Pirat, Muriel Richard-Noca, Christophe Paccolat, Volker GassVolker Gass. Mission Design and GNC for In-Orbit Demonstration of Active Debris Removal Technologies with CubeSats. *Acta Astronautica*, 2016.

[3] Vladimir A. Chobotov. *Orbital Mechanics, Third Edition*. American Institute of Aeronautics and Astronautics, Inc., January 2002.

[4] Grant H. Stokes,Curt von Braun, et al. The space-based visible program. *Lincoln Laboratory Journal, Vol. 11,No. 2*, 1998.

[5] Laila Kazemi, Alexander Vandenberghe, Mikel Samson, Bram Vandoren, Tjorven Delabie. Debris Detection Using Star Tracker Concept Verification. *Small Satellite Conference*, 2024.

[6] Oliver Montenbruck and Eberhard Gill. *Satellite Orbits*. Springer Berlin Heidelberg, 2000.

[7] Rauno Gordon, Alar Leibak, Peeter Orgb. ADCS development for student CubeSat satellites – TalTech case study. *Proceedings of the Estonian Academy of Sciences*, 2021.

[8] J. Sharma, C. von Braun, and E. M. Gaposchkin. Space-based visible data reduction. *Journal of Guidance, Control, and Dynamics*, 23(1):170–174, January 2000.

[9] T. Flohrer, J. Peltonen et al. Space based optical observations of space debris. *4th European Conference on Space Debris,ESA*, 2005.

[10] Utzmann J,Wagner A, et al. A system design for space-based space surveillance. *Small Satellites Systems and Services (The 4S) Symposium*, 2014.